Title: Acidification in coastal waters of Adélie Land, Antarctica (1985-2025)

Nicolas Metzl[1], Bronte Tilbrook[2,3], John Akl[2], Craig Neill[2], Alexandra Aymard[1], Claire Lo Monaco[1], Gilles Reverdin[1], Jean-Baptiste Sallée[1], Aude Barton[4], Frédéric Chevallier[4], Marion Gehlen[4]

1 Laboratoire LOCEAN/IPSL, Sorbonne Université-CNRS-IRD-MNHN, Paris, 75005, France
2 CSIRO Environment, Castray Esplanade, Hobart, TAS 7004, Australia
3 Australian Antarctic Partnership Program, University of Tasmania, Hobart, TAS, Australia
4 Laboratoire LSCE/IPSL, CEA-CNRS-UVSQ, Université Paris-Saclay Gif-sur-Yvette, 91191, France

Correspondence to: Nicolas Metzl (nicolas.metzl@locean.ipsl.fr)

Keywords: Acidification, Air-Sea CO_2 fluxes, Southern Ocean, Coastal, Adélie Land

Abstract:

Ocean acidification is expected to be particularly severe in Antarctic continental shelves due to enhanced anthropogenic carbon uptake in cold waters in response to rising atmospheric CO_2, sea-ice retreat, freshening and climate-change feedbacks. Models suggest that undersaturated conditions with respect to aragonite (Ω_{ar}), a major form of calcium carbonate formed by marine species, could be reached as soon as 2052 for austral winter. Here we present new ocean carbonate system observations from cruises conducted since 2010 in the Adélie Land coastal region in East Antarctica, along with data from a BCG-Argo float and results from a neural network model for the period 1985-2025. The region is a permanent CO_2 sink which was most pronounced since 2006. The CO_2 sink leads to an increase of surface water total CO2 concentrations (C_T) (+0.44 ± 0.01 µmol kg^{-1} yr^{-1}) and to a decrease of pH (-0.013 per decade) and Ω_{ar} (-0.035 per decade) for the winter season. The lowest surface Ω_{ar} of 1.2 was observed in winter 2024 from the float data, a critical limit for some marine species such as pteropods. A projection of the C_T concentrations in the future, based on observed anthropogenic CO_2 concentrations and emissions scenarios, suggests that aragonite saturation state (Ω_{ar} = 1) will occur in surface waters as soon as 2055 in the Adélie Land region, which is part of a larger area of East Antarctica proposed as a Marine Protected Area by the Commission for the Conservation of Antarctic Marine Living Resources since the early 2010s.

1 Introduction

Coastal and continental shelf waters can experience ocean acidification (OA) due to increasing ocean CO_2 uptake in response to increased greenhouse forcing (Bourgeois et al 2016; Laruelle et al, 2018; Roobaert et al, 2024a,b). As opposed to the open ocean, the detection of CO_2 and acidification trends in Antarctic coastal waters is complicated by multiple effects such as anthropogenic CO_2 (C_{ant}) uptake, warming or cooling, variability in biological processes, upwelling, and changes in sea-ice cover and freshening.

In the Southern Ocean, OA has been studied using sea surface CO_2 fugacity (fCO_2) observations at regional scale mainly in the Sub-Antarctic, Polar Front or Permanent Open Ocean zones (Xue et al 2018; Brandon et al 2022; Metzl et al 2024b). There are two long-term time series in the Drake Passage to the north of the Antarctic Peninsula (Takahashi et al, 2014; Hauri et al 2015; Munro et al, 2015) that have been used to evaluate OA in coastal Antarctic zones. The observed pH rates at Drake and Palmer station ranged between +0.020 ± 0.020 and -0.015 ± 0.008 $decade^{-1}$.

Recently, Mazloff et al (2023) merged Biogeochemical Argo (BGC-Argo) float and historical observations to estimate OA in the entire Southern Ocean (SO). In the seasonal ice zone (SIZ), they evaluated pH trend of -0.0242 ± 0.0007 decade^{-1} between 1994 and 2017 in subsurface waters (100-210m). Estimates of the decadal change in OA based on observations, are often limited to data collected 2 to 15 years apart (e.g., Hauck et al 2010; Pardo et al 2017; Carter et al 2019). In the regions of dense water formation, C_{ant} is efficiently transported to the deep ocean implying that acidification can be detected not only in surface waters but also in deep and bottom waters (Zhang et al, 2023). The Adélie Land region is one of the four main bottom water formation regions in Antarctica with the formation of Adélie Land Bottom Water (ALBW), which was first recognized by Gordon and Tchernia (1972). Subsequently, a number of studies have described and quantified the variability of the ALBW formation and its properties (e.g. Williams et al, 2010; Aoki et al, 2013; van Wijk and Rintoul 2014; Shadwick et al, 2014; Pardo et al 2017). Once formed on the continental shelf and slope, ALBW is transported away from its source, and ventilates the entire Australian-Antarctic Basin and beyond (Sholeninova et al, 2025). Significant C_{ant} concentrations of up to 44 µmol kg^{-1} have been observed in the shelf waters (Shadwick et al, 2014), linking the ocean CO_2 uptake in coastal waters and OA at depth (Zhang et al, 2023)

The Adélie Land is part of a proposed Marine Protected Area of East Antarctica (Boothroyd et al, 2024) and severe undersaturated conditions with respect to aragonite could occur as soon as 2055 at the surface in austral winter and in 2080 for summer (Nissen et al, 2024). Preliminary results based on summer observations gathered from 2002 to 2012 indicate that the trend of surface water total CO_2 concentrations (C_T) in the Adélie Land region was not significant (N-C_T trend = +0.63 ± 0.70 µmol kg^{-1} yr^{-1}, Metzl et al 2025a). This region has large inter-annual variability in pCO_2 and C_T linked to competitive processes between anthropogenic CO_2 uptake, primary production, mixing, or ice melting (Shadwick et al., 2013, 2014, 2017) possibly masking the trend.

In this context, more data are needed to better evaluate the changes in the carbonate system in Antarctic coastal zones and the associated OA (Tilbrook et al, 2019). This would allow us to better evaluate the long-term changes with regard to the biological impacts and offer better validation for ocean and Earth system models that struggle to reproduce the seasonal cycles of the carbonate chemistry and remain poorly constrained to project future OA changes, particularly in high latitudes.

In this study, we present new fCO_2 and C_T data obtained in January 2024 and in December-February 2024-2025 off Adélie Land region combined with historical data and machine learning products to better define the seasonality and trends in C_T and OA. Using historical data since the 1980s and BGC-Argo float data in 2024-2025 we estimate the trends in the carbonate system (pH and Ω_{ar}). As most observations were obtained in austral summer (December-March) the results from a reconstruction of the global surface ocean carbonate system model (Chau et al, 2024a) that extended to 2025 were used to explore the decadal trends for different seasons. Based on subsurface anthropogenic CO_2 concentrations estimates for 1995 to 2025 we investigate future changes in Ω_{ar}. Previous studies predicted undersaturation with respect to aragonite to be reach by the mid of this century (Nissen et al., 2024) with potential detrimental impacts for marine calcifiers such as pteropods (Bednaršek et al., 2023).

2 Data selection and methods

2.1 Data selection in the Adélie Land sector

To explore the long-term change of the carbonate system in this region, we selected the fCO_2 data from Surface Ocean CO_2 Atlas (SOCAT), version v2025 (Bakker et al, 2016, 2025) with the addition of 3 recent cruises conducted on-board the ship L'Astrolabe in December 2024, January 2025 and February 2025. These include 67 cruises from 1984 to 2025 south of 63°S and between 140-150°E (see the detail in Supplementary Material Table S1 and Figure 1). During some cruises (MINERVE cruises between 2003 and 2012 and OISO-10 cruise in 2003) continuous underway or regular sampling for total alkalinity (A_T) and C_T measurements were performed (data available in the SNAPO-CO2 data-set, Metzl et al, 2025a). During the L'Astrolabe cruise in January 2025, A_T and C_T samples in sea surface water were also taken, analyzed at the SNAPO-CO2 service facilities at LOCEAN laboratory (Paris/France), and included in this work. In addition, we also used water column data between 1993 and 2018 from the Global Ocean Data Analysis Project (GLODAP), version GLODAPv2.2023 data-base (Lauvset et al, 2023, 2024; Supplementary Material Table S2); the GLODAP data in surface waters (0-30m) are also used to synthetize all A_T and C_T data in the region and used to validate and compare results of the C_T and pH trends based on fCO_2 data and to complement periods when fCO_2 data are not available. Finally, data from a BGC-Argo float in 2024-2025 (WMO 2903867) are introduced to complement the water column and winter data.

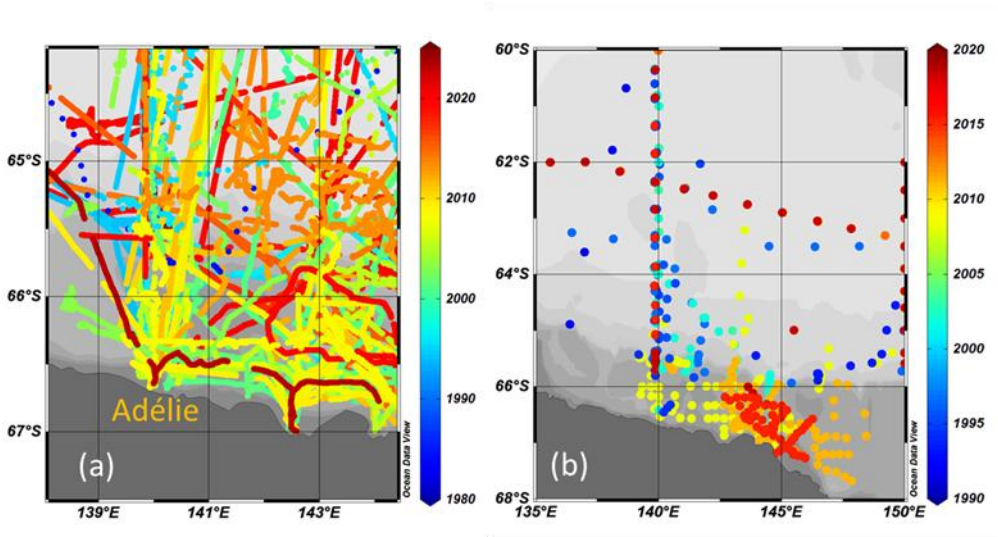


Figure 1: Maps of (a) SOCAT data and (b) GLODAP data selected in the Adélie Land region. Color code is for year. Figures produced with ODV (Schlitzer, 2018).

2.2 Methods

The methods to derive surface underway fCO_2 in SOCAT were described in previous studies (e. g. Metzl et al, 1999; Ishii et al, 2002; Brévière et al, 2006; Laika et al, 2009; Midorikawa et al 2012; Shadwick et al 2014 & 2017), or detailed in the cruises metadata available in the SOCAT data-sets (www.socat.info). The methods for underway or discrete A_T and C_T measurements were described and available in the SNAPO-CO2 data-set (Metzl et al, 2024a; 2025a). Here we describe the methods used during the L'Astrolabe 2024-2025 cruises.

The underway fCO_2 measurements onboard L'Astrolabe in December 2024/February 2025 (Supplementary Material Figure S1) were made by CSIRO, Hobart, using a General Oceanics 8050 fCO_2 system equipped with a LICOR LI-7815 analyser (Pierrot et al, 2009; Tilbrook et al, 2025). The

same technique was used during Le Commandant Charcot voyage in 2023 and Investigator voyage in 2024. The precision of the fCO_2 data is estimated to be ±2 µatm, with cruises flagged B in SOCAT (Supplementary Material Table S1, Gkritzalis et al, 2024).

In December 2024-January 2025, discrete sampling was performed from the ship's seawater supply for salinity, A_T, C_T, $\delta^{13}C$, $\delta^{18}O$. Salinity is given on the practical salinity scale (UNESCO, 1981). For A_T and C_T samples were collected in 500 mL borosilicate glass bottles and poisoned with 300 µL of $HgCl_2$, closed with greased stoppers (Apiezon®) following the standard operating procedures of Dickson et al. (2007). Discrete samples were returned to the LOCEAN laboratory (Paris, France) in March 2025, stored in a dark room at 4 °C, and analyzed in April 2025. A_T and C_T were measured using a potentiometric titration method (Edmond, 1970) in a closed cell. For calibration, we used the Certified Referenced Materials (CRM # 208) provided by Prof. A. Dickson (SIO, University of California). A total of 31 samples were analyzed for the R2 cruise in December 2024-January 2025. Two anomalous values were identified for both A_T and C_T (WOCE flag 4 assigned) either due to a sampling or analytical issues and were not considered further (Supplementary Material Figure S2). For the other data, we estimate that the accuracy for both A_T and C_T is better than 4 µmol kg^{-1}, as for other samples measured at the SNAPO-CO2 facilities (Metzl et al, 2025a). These data were used for the validation of calculated carbonate system parameters using fCO_2 data with an A_T/salinity relationship.

In this region a BGC-Argo float (WMO 2903867) was launched on 26 January 2024 at location 132°E/64°S and drifted south-eastward. Like other SOCCOM floats (Sarmiento et al, 2023) this float recorded T, S, O_2, pH, nitrates and Chl-a down to 1500m. The float data are available at https://www.mbari.org/products/data-repository/, last access 10 May 2025). Its last record with good pH data was on 15 January 2025 at 144.5°E/66.2°S. A_T was estimated with the LIAR V2.2 algorithm (Carter et al., 2016, 2017). From pH and A_T data we calculated C_T, Ω_{ar} and fCO_2 using the same CO2sys code used for the shipboard data (section 2.3). Based on the uncertainty of the float data and calculations the C_T, fCO_2 and Ω_{ar} errors are respectively of 6.8 µmol kg^{-1}, 9.4 µatm and 0.103.

2.3 Carbonate system calculation and A_T/Salinity relationship

From fCO_2 or A_T and C_T data, we calculated pH_T (pH at total scale) and the saturation states of aragonite and calcite (Ω_{ar}, Ω_{ca}). Here we used the CO2sys program (version CO2sys_v2.5, Orr et al., 2018) with K_1 and K_2 dissociation constants from Lueker et al. (2000), KSO_4 dissociation constant from Dickson (1990). Total boron concentration was calculated according to Uppström (1974). Nutrients were not measured for many cruises and when not available we used fixed climatological values of 40 and 2 µmol kg^{-1} for silicate and phosphate respectively (Supplementary Material Figure S3; Beucher et al, 2004; Bender et al, 2016). When a strong bloom occurred, as indicated by high fluorescence and low fCO_2, the nutrient concentrations were halved. The nutrient values used had no impact on the long-term trends. When using fCO_2 data to derive pH_T, C_T, or Ω_{ar}, the A_T concentrations are derived from salinity (e.g. Millero et al, 1998; Lee et al, 2006; Shadwick et al, 2014; Stark et al, 2018; Leseurre et al, 2022). Here we used the A_T/Salinity relationship derived from A_T data south of 60°S (Supplementary Material Figure S4).

A_T (µmol kg^{-1}) = 53.8059 (± 1.022) x Salinity + 467.985 (± 34.600), (r2 = 0.48, n= 2992) (Eq. 1)

This relation compared well with those previously estimated in the southern ocean (Lee et al 2006; Shadwick et al, 2014; Stark et al, 2018) as well as when derived from GLODAP data only (Supplementary Material Figure S4). This relation has been checked for the region south of 63°S, i.e. south of the nutrients gradient (Figure S3) and will be used for the trend analysis discussed in section 3.3.

To take into account the warming/cooling or the freshening, the fCO_2 and C_T data were also normalized. For temperature fCO_2 normalization (fCO_2^n) at SST fixed (SST_{fix}) we used the relation described by Takahashi et al (1993):

$$fCO_2^n = fCO_2 \, EXP(0.0423*(SST_{fix}-SST))$$

The salinity C_T normalization was calculated at salinity 34 ($N\text{-}C_T = C_T \times 34/SSS$).

2.4. Observation-based reconstructions of surface ocean carbonate system variables

Output from CMEMS-LSCE-FFNN, an ensemble-based feed-forward neural network (CMEMS-LSCE-FFNN or FFNN for simplicity, Chau et al, 2024a) at global scale and 0.25°x0.25° resolution provided fCO_2 for seasons when direct observations were not available. Precisely, an ensemble of 100 models was trained on randomly subsampled SOCAT and predictor data with a ratio of 2:1 for training and validation. The approach uses a 3-month gliding window and the month of reconstruction is excluded from the training data (p-leave out). The means (μ) and standard deviations (σ) are computed from the 100-member ensembles and represent the model best estimate and associated uncertainty. The predictors include sea-surface height, sea surface temperature, sea surface salinity, mixed-layer depth, chlorophyll-a, atmospheric CO_2 and geographical coordinates (longitudes and latitudes) as well as pCO_2 from the climatology (Takahashi et al, 2009). The model uses fCO_2 data from SOCATv2025 (Bakker et al, 2025) that covers January 1985 to December 2024, while 2025 is produced in near-real-time (NRT) prediction mode (Chau et al, 2024b). The reconstructed fCO_2 field for 1985-2025 was used to derive air-sea CO_2 fluxes. Time and space varying surface total alkalinity fields, A_T, were derived from the multivariate linear regression model LIAR (Carter et al., 2016; 2017) based on sea surface temperature, salinity, and nutrients concentration (nitrate, silicate, from WOA18, Garcia et al, 2019), i.e. the same as for BGC-Argo floats. Surface ocean pH and C_T were obtained from reconstructed fCO_2 and A_T, temperature, salinity, and nutrients through the speciation software CO2sys. Uncertainty of pH, A_T and C_T is derived from LIAR and CO2sys error propagation (Orr et al. 2018) at each grid cell and for each time step. For the in-depth evaluation of fCO_2, pH, A_T and C_T please refer to Chau et al. (2022, 2024a). Note the no specific tuning was employed for the region under study. When comparing the C_T or pH trends from the model based on A_T derived from LIAR or from Eq. 1 we obtained the same results (Supplementary Material Table S3). The multi-year reconstruction and the near-real time prediction, including uncertainty estimates, are available under the DOI https://doi.org/10.48670/moi-00047 (last access, 9 August 2026).

3 Results and discussion

3.1 Air-sea CO2 fluxes

To investigate the temporal changes of the air-sea CO_2 fluxes we used the model results in the region 65-66.5°S/139-141°E after averaging the monthly 0.25x0.25 grid cells in this box. During the first period, 1985-2000, the FFNN model estimated a CO_2 flux close to 0 (average = -0.030 ± 0.107 molC m^{-2} yr^{-1}). After 2000, the model suggests an increase of the CO_2 sink especially after 2016

(Figure 2), a signal identified at a larger scale in the Antarctic Seasonal Ice Zone in Spring-Summer 2003-2022 (Deng et al, 2025). The maximum CO_2 sink of -1.2 molC m^{-2} yr^{-1} occurred in 2023. This is much stronger than the flux of -0.31 molC m^{-2} yr^{-1} derived from the climatology in 2010 (Fay et al, 2024). In austral summer, the variability of the flux could be large. Previous studies reported fluxes ranging between +0.1 to -3.5 mmolC m^{-2} d^{-1} in summer in this region (Ishii et al, 2002; Arroyo et al 2020) but the CO_2 sink could be up to -15 to -30 mmolC m^{-2} d^{-1} in the Mertz Polynya region east of the Adélie Land (Shadwick et al 2014; 2017). In January 2023 the sink derived from the FFNN model reached a maximum of -17 mmolC m^{-2} d^{-1}. This was associated to low fCO_2 (321.5 µatm) and high wind speed (up to 7.8 $m.s^{-1}$) during a high positive Southern Annual Mode (SAM index of 4.56 in January 2023, data obtained from https://legacy.bas.ac.uk/met/gjma/sam.html, last access 29 Oct. 2025, based on Marshall (2003)). Strong CO_2 sinks, < -10 mmolC m^{-2} d^{-1}, were also estimated in January 2019 and in February 2002, 2016 and 2021 also associated to positive SAM (>1.4). In January and February 2025, the period of the L'Astrolabe recent cruises, the sink was respectively -7.6 ± 2.9 and -12.1 ± 6.1 mmolC m^{-2} d^{-1} (when the SAM was respectively only 1.4 and 0.31). The impact of the CO_2 uptake and its increase over time on the pH_T and Ω_{ar} changes is discussed in the following sections.

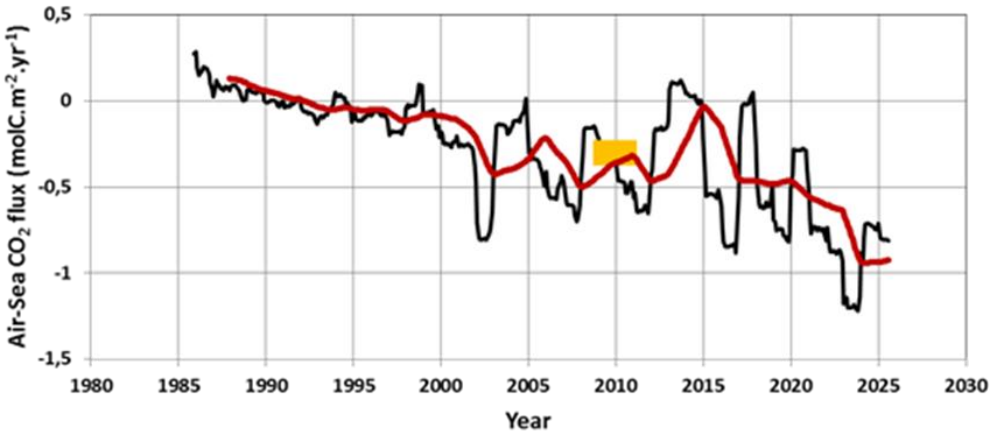


Figure 2: Time-series of air-sea CO_2 flux (annual in black, 36-month running mean in red) in the Adélie Land region based on the FFNN-LSCE model over 1985-2025 (centered at 66°S/140°E). Also shown (Orange Square) the climatological flux for year 2010 at the same location (Fay et al, 2024). Negative value denotes ocean CO_2 sink.

3.2 Recent cruises and a BGC-Argo float (2024-2025)

The 2024-2025 shipboard and BGC-Argo observations consistently showed the ocean was a CO_2 sink in summer (Figure 3). The large spatial variability observed at 66-67°S, with fCO_2 lower than 300 µatm, was linked to biological activity concentrated near the coast above the Adélie Bank (140-142°E) and the Mertz Bank (145-147°E) (Supplementary Material Figure S5). Biological processes also drove significant inter-annual changes. For example, along the ~140°E track visited in January 2024 (RV/Investigator) and in February 2025 (L'Astrolabe), fCO_2 showed the same southward decrease but shifted by 26 µatm, while only 7 µatm is attributable to the temperature differences (Figure 4a). The C_T concentrations derived from the fCO_2 data indicated that the difference was most pronounced at 65.3°S (Figure 4b) where the Chl-a was higher in 2024 (Supplementary Material Figure S5). This

demonstrates that biology drives most spatial and temporal variability making C_T or pH_T trend detection difficult in Antarctic coastal summer data (Monteiro et al, 2020; Metzl et al, 2025a).

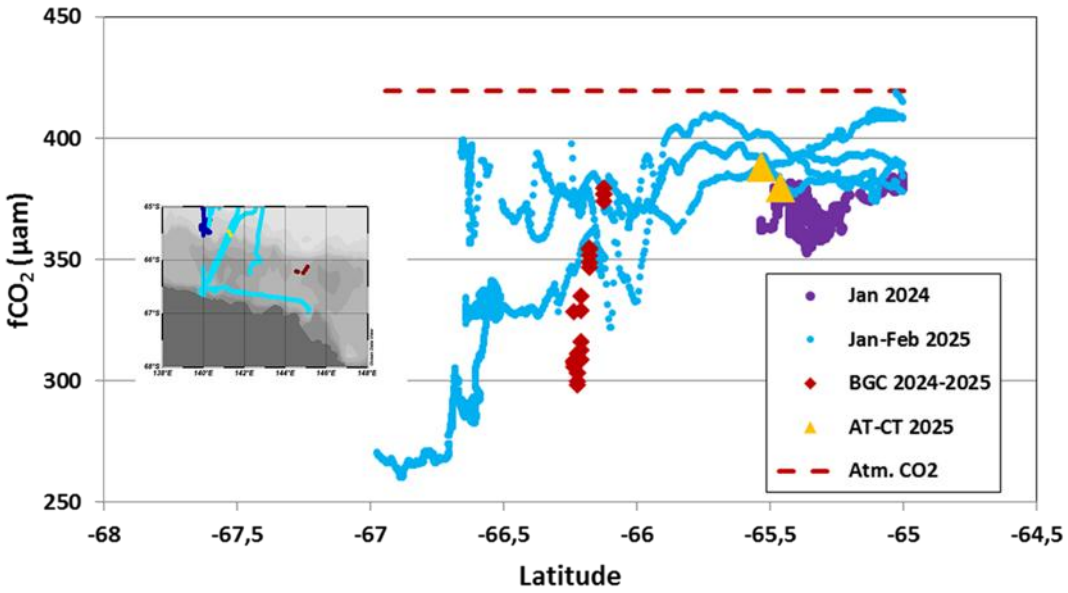


Figure 3: Distribution of sea surface fCO_2 (µatm) observed south of 65°S in January 2024 (purple) and January-February 2025 (blue) from shipboard, in December 2024 and January 2025 from the BGC-Argo (red diamonds), and calculated from A_T C_T data in January 2025 (orange triangles). The red dashed line is the mean atmospheric fCO_2 in January 2025 at Cap Grim or at South Pole (419.5 µatm). (https://gml.noaa.gov/dv/iadv/). Locations of the data are identified in the insert map produced with ODV (Schlitzer, 2018).

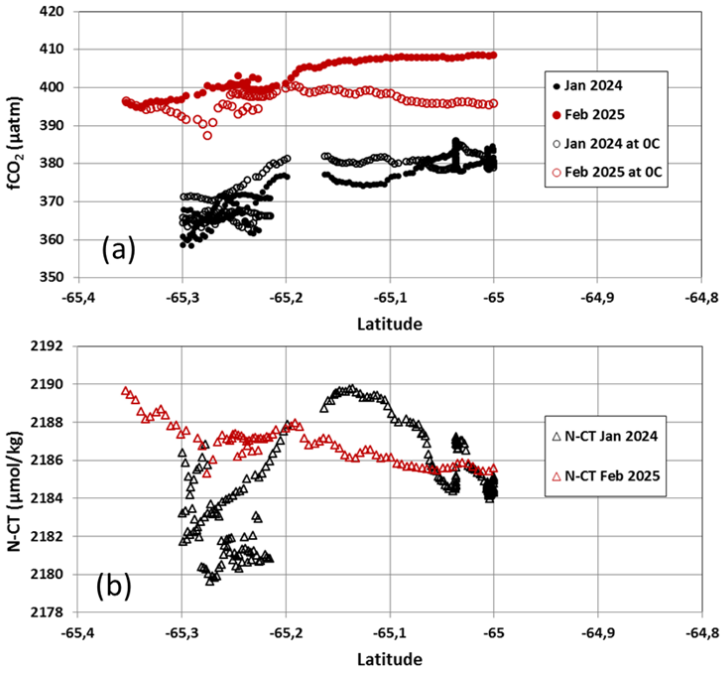


Figure 4: (a) Distribution of sea surface fCO_2 (µatm) and temperature normalized fCO_2 at 0°C (open symbols) observed south of 65°S in January 2024 (black) and February 2025 (red) along the same track. (b) Same as (a) for salinity normalized C_T concentrations (µmol kg^{-1}) calculated from fCO_2 data.

The low N-C_T in 2024 (< 2182 µmol kg^{-1}) were linked to higher biological activity in 2024 (Figure S5 in Supp. Mat.).

A BGC-Argo float (WMO 2903867) provided wintertime fCO_2 data for 2024 (Figure 5). The maximum fCO_2 of 440 µatm, above the atmospheric CO_2 level, occurred in September (Figure 5a). In September 2024, and given the error associated to the fCO_2 data derived from the float (± 9.4 µatm), we estimated a positive ocean-atmosphere difference (ΔfCO_2 > 0, a potential CO_2 source) with a range between 28.4 and 9.6 µatm. The FFNN model also produced a maximum of fCO_2 in winter (fCO_2 = 427 µatm in August 2024, Figure S6) leading to a wintertime CO_2 source of 0.43 mmolC m^{-2} d^{-1}. In August 1996 during the only cruise conducted in austral winter (Expocode 09AR19960822) we estimated fCO_2 from the A_T C_T data in surface waters. This also lead to a potential CO_2 source, ΔfCO_2 ranging between 31.7 and 7.5 µatm. For the same periods, August 1996 and September 2024, ΔfCO_2 from the FFNN model were respectively 37.95 and 12.4 µatm. The air-sea CO_2 fluxes estimated by the FFNN model were +0.176 mmol C m^{-2} d^{-1} in August 1996 and + 0.184 mmol C m^{-2} d^{-1} in September 2024, i.e. a similar value observed 28 years apart.

In September 2024 the sea surface C_T estimate from the float reached a maximum of 2221.3 ± 1.9 µmol kg^{-1} compared to 2207.2 ± 3.7 µmol kg^{-1} measured in August 1996 (Figure 5b). The difference of +14.1 µmol kg^{-1} would translate into a rate of +0.5 µmol kg^{-1} yr^{-1} over 28 years similar to the range of the anthropogenic CO_2 trend in the Antarctic Surface Water (AASW), +0.35 ± 0.14 to +0.65 ± 0.21 µmol kg^{-1} yr^{-1} derived from 4 cruises in 1995-2011 in this region (Pardo et al, 2017). Consequently, pH_T decreased from 8.054 ±0.005 (winter 1996) to 7.976 ± 0.002 (winter 2024) (Figure 5c) and Ω_{ar} decreased from 1.334 ± 0.017 to 1.157 ± 0.009 (Figure 5d). A pH_T decrease of 0.0781 in 28 years corresponds to a trend of -0.028 per decade. This substantial signal derived from measured pH (BGC-Argo in 2024) and calculated pH_T (shipboard A_T and C_T data in 1996), is sensitive to method uncertainties. Accounting for A_T and C_T measurements uncertainty (± 4 µmol kg^{-1}, Lauvset et al, 2024) the pH_T decrease ranges from -0.021 to -0.035 per decade consistent with previous estimates of -0.035 ± 0.002 per decade in the AASW in this region (Pardo et al, 2017). This rapid pH_T decrease requires confirmation with longer time series and quantification of contributing processes (anthropogenic CO_2 signal, mixing, warm deep water intrusion, sea-ice extent, natural variability…).

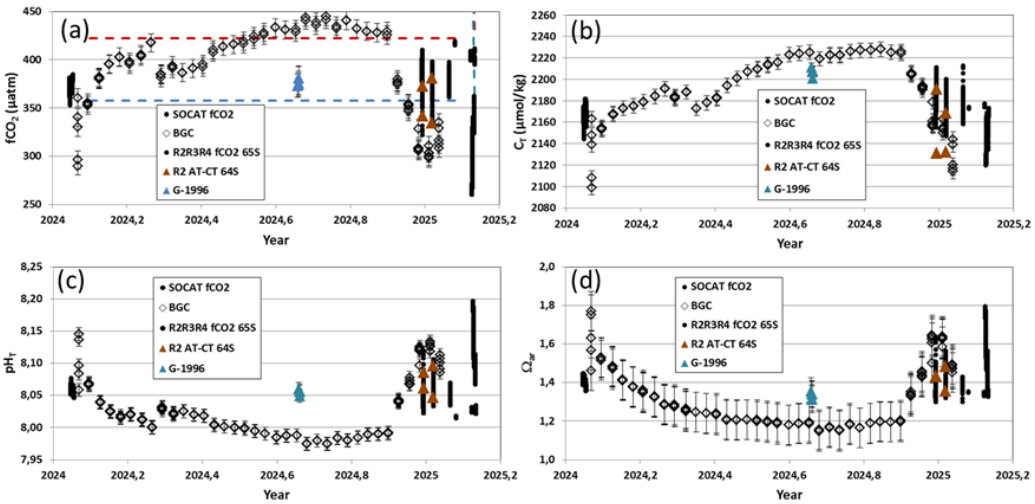


Figure 5: Time-series of (a) sea surface fCO_2 (µatm), (b) C_T (µmol kg^{-1}), (c) pH_T and (d) Ω_{ar} observed south of 64°S in 2024-2025 based on SOCAT fCO_2 data (black circles), L'Astrolabe fCO_2 data (R2R3R4,

black circles), BGC-Argo float (open diamonds) and A_T C_T data in January 2025 (R2, orange triangles). Also shown the results from A_T C_T data from a cruise in winter 1996 (blue triangles, cruise 09AR19960822). The dashed lines in (a) are the mean atmospheric CO_2 concentrations in 1996 (blue) and 2025 (red). Error bars (vertical) are indicated for measured or calculated values.

3.3 The period 1985-2025: high variability in summer, trends in winter

To evaluate trends we averaged data from each cruise around 140°E and south of 65°S. In this region fCO_2 data from SOCAT are available since 1984 and A_T and C_T data from GLODAP and SNAPO-CO2 since 1994. The FFNN model starts in 1985 and was constrained by satellite Chl-a data since 1998, and by climatological Chl-a before then.

The average fCO_2 and C_T data present higher values in recent years (Figure 6). The fCO_2 average for January 2025 (mean = 382.3 µatm) was much higher than the first data in January 1984 (fCO_2 = 317.5 µatm). The difference of 64.8 µatm would translate into a trend of +1.58 µatm yr^{-1} with the atmospheric trend of +1.98 ppm yr^{-1} for the same period. In January 2025, the C_T measurements (C_T normalized at salinity 34, N-C_T = 2182 µmol kg^{-1}) increased by +10 µmol.kg^{-1} compared to January 1994 (N-C_T = 2172 µmol kg^{-1}) corresponding to a trend of +0.32 µmol kg^{-1} yr^{-1}.

Although the C_T data present higher concentrations in the recent decade, the trends based on observations are uncertain due to the large inter-annual variability (Table 1). Indeed, the time series of fCO_2 and C_T present large inter-annual variability in summer (Figure 6) which is particularly apparent in 2002 and 2015 and was clearly linked to biological activity (Supplementary Material Figures S7, S8). The FFNN model captured these anomalies leading to stronger CO_2 sinks in summer 2002 and 2015 (Figure 2, Supplementary Material Figure S8). This also led to anomalies in pH_T and Ω_{ar} (Figure 7). Consequently, the long-term trends of observed properties in summer are uncertain and the errors associated with the trends in the FFNN model are also larger in summer compared to winter (Table 1). A simple linear projection of the Ω_{ar} trend in winter from the FFNN model (-0.0035 ± 0.0001 yr^{-1}) suggests that a value of 1.2 would be reached in 2032 and saturation (Ω_{ar}=1) in 2090.

Table 1: Trends of properties in the Adélie zone derived from observations (measured A_T, C_T or fCO_2) and from the FFNN model. For observations the trends are evaluated for summer only. For the FFNN model trends are estimated for all seasons or only for January and August. The last line is based on winter data in 2024 (BGC-Argo) and 1996 (A_T C_T data). Standard-deviations are in brackets.

Method	Period	fCO_2 µatm yr^{-1}	A_T µmol kg yr^{-1}	C_T	pH_T yr^{-1}	Ωar yr^{-1}
A_T C_T 1995-2025		0.14	-0.11	0.00	-0.0002	-0.0010
Summer		(0.66)	(0.38)	(0.36)	(0.0008)	(0.0027)
fCO_2 1984-2025		1.33	0.04	0.50	-0.0015	-0.0040
Summer		(0.33)	(0.25)	(0.24)	(0.0004)	(0.0011)
FFNN 1985-2025		0.58	-0.29	0.08	-0.0007	-0.0031
Summer		(0.23)	(0.08)	(0.15)	(0.0003)	(0.0010)
FFNN 1985-2025		1.33	-0.002	0.44	-0.0013	-0.0035
Winter		(0.04)	(0.007)	(0.01)	(0.0001)	(0.0001)
FFNN 1985-2024		1.27	-0.05	0.44	-0.0013	-0.0040
Annual		(0.09)	(0.04)	(0.08)	(0.0001)	(0.0003)
BGC-Argo versus A_T C_T		2.28	-0.27	0.50	-0.0028	-0.0063

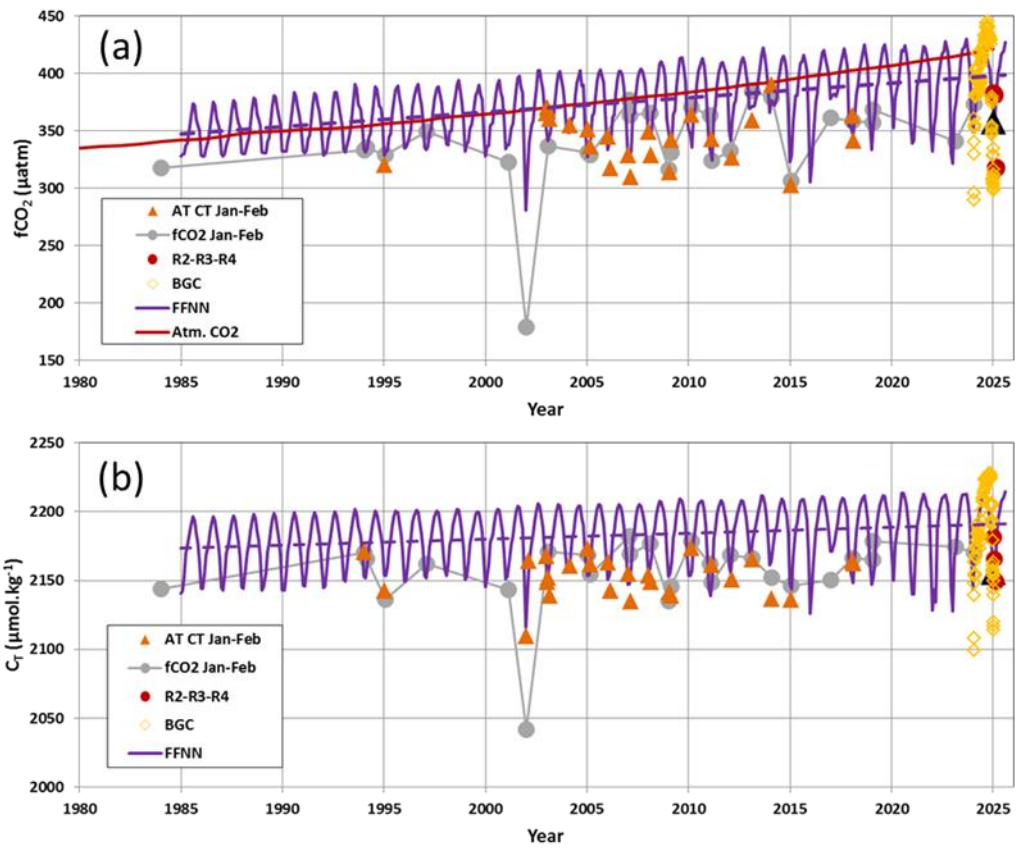


Figure 6: Time-series of (a) sea surface fCO_2 (µatm) and (b) C_T (µmol kg^{-1}) observed south of 65°S based on SOCAT fCO_2 data in summer 1985-2024 (grey circles), from A_T C_T data in summer 1995-2018 (orange triangles), L'Astrolabe fCO_2 data in summer 2025 (R2R3R4, red circles), A_T C_T data in 2025 (R2, black triangles) and BGC-Argo float data in 2024-2025 (open diamonds). Also shown are the monthly values of the FFNN model (purple) and the associated trend (dashed lines, +1.27 µatm yr^{-1} and 0.44 µmol kg^{-1} yr^{-1}). In (a) the red line is the atmospheric fCO_2.

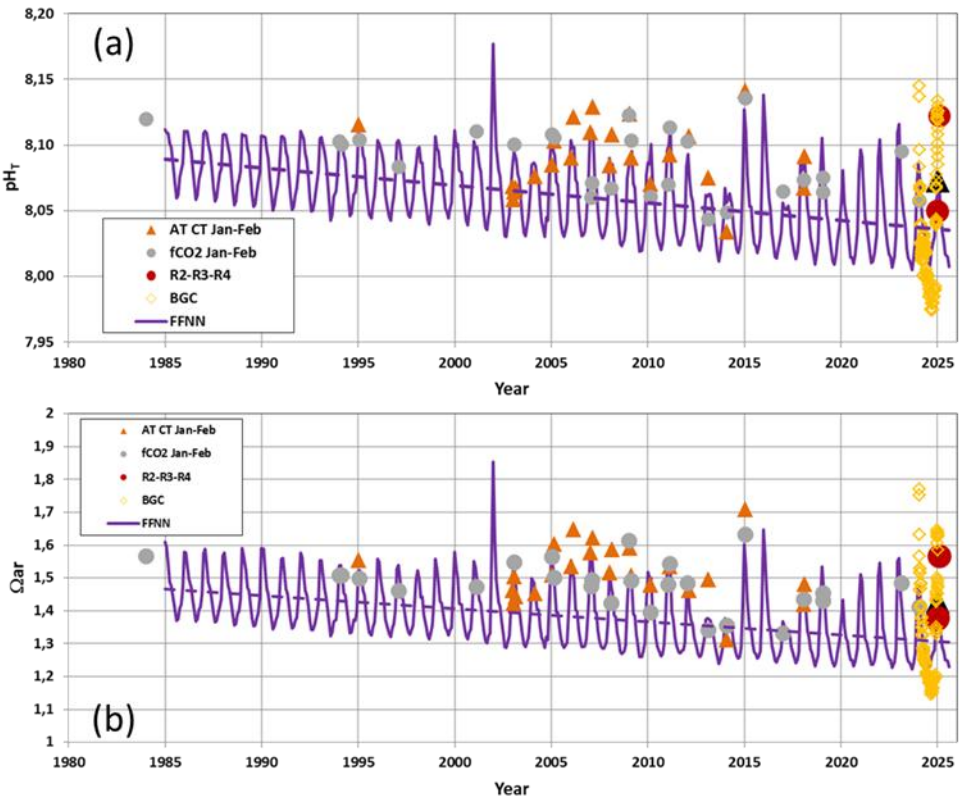


Figure 7: Time-series of (a) pH_T and (b) Ω_{ar} observed south of 65°S based on SOCAT fCO_2 data in summer 1984-2024 (grey circles), from A_T C_T data in summer 1995-2018 (orange triangles), L'Astrolabe fCO_2 data in summer 2025 (R2R3R4, red circles), A_T C_T data in 2025 (R2, black triangles) and BGC-Argo float data in 2024-2025 (open diamonds). Also shown are the monthly values of the FFNN model (purple) and the associated trend (dashed lines, see Table 3, pH= -0.0013 yr^{-1} and Ω_{ar} =-0.0040 yr^{-1}).

The observations indicate that the lowest Ω_{ar} occurred in winter 2024 (BGC-Argo data, Ω_{ar} = 1.146, on 6 September 2024). This is 0.25 lower than in 1985 and 0.15 lower than in 1996 and the decrease of Ω_{ar} in surface also occurred at depth (Figure 8). In the mixed layer Ω_{ar} decreased from around 1.35 in August 1996 to 1.15 in winter 2024. Such a value is observed at 200m in January 2025 and at 300-400m in 1996 indicating an upward migration of Ω_{ar} (Pardo et al, 2017). We noticed that the FFNN value in August 1996 (Ω_{ar} = 1.34) was coherent with that observed in August 1996 in the mixed-layer (Figure 8). In August 2024 and 2025, the FFNN value (Ω_{ar} = 1.23) is close to that observed from the float in winter 2024 (Ω_{ar} = 1.2) and to the data observed at 200 m in 1996 or at 75 m in 2025. The distribution of Ω_{ar} for the FFNN is more homogeneous in winter (Supplementary Material Figure S9) and provides a smaller error estimate of the long term trend but is constrained by few observations. The FFNN model also has a more variable air-sea CO_2 flux during summer compared to

winter (Supplementary Material Figure S10), leading to significant change in annual CO_2 uptake (Figure 2). The seasonal amplitude from the FFNN results also show significant variability over 5-10 years after 1998 (Supplementary Material Figure S11) but no trend of the fCO_2 seasonality was detected as was suggested in other ocean regions (e.g. Landschützer et al., 2018; Rodgers et al., 2023; Shadwick et al 2023). To estimate the processes that drive the pH_T and Ω_{ar} changes we focus on results for the winter season.

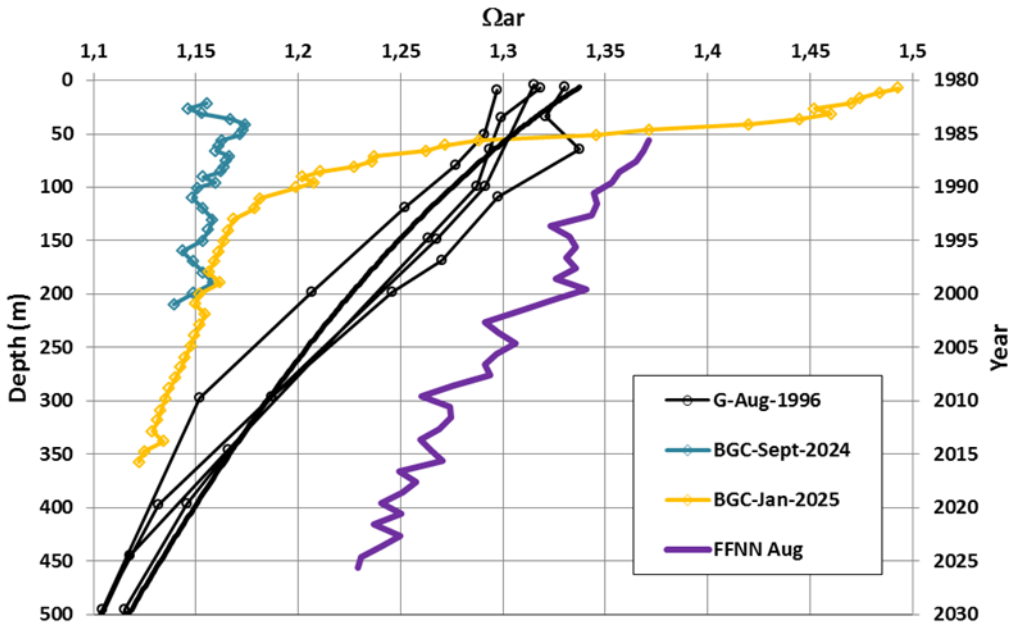


Figure 8: Profiles (0-500m left axis) of Ω_{ar} in August 1996 (GLODAP data, black circles), September 2024 (BGC-Argo, blue diamonds) and January 2025 (BGC-Argo, orange diamonds) along with surface time-series in 1985-2025 (right axis) of Ω_{ar} in August from the FFNN model (purple line). In the mixed layer Ω_{ar} decreased from around 1.35 in 1996 to 1.15 in 2024 (i.e. a value observed at 300-400m in 1996). The FFNN values in August 1996 are coherent with August 1996 observations in the mixed-layer. In August 2025, Ω_{ar} FFNN value of 1.23 is close to the data observed at 200m in 1996 or at 75m in 2025 demonstrating the upward shift of Ω_{ar}.

3.4 Anthropogenic CO_2

To estimate the anthropogenic CO_2 concentrations (C_{ant}) in the water column we used the TrOCA method developed by Touratier et al. (2007). This method was successfully used in the southern Ocean (Shadwick et al, 2014; Kerr et al, 2018; Mahieu et al., 2020; Zhang et al, 2023; Metzl et al, 2024b). Here we selected the data below 100m depth for 1994-2018 and from the BGC-Argo float (March 2024 to January 2025, Supplementary Material Figure S12). The C_{ant} trends were tested in three layers, 100-150 m, 150-200 m and 200-250 m (Figure 9). In all layers, the mean C_{ant} concentration ranged from 15-25 µmol.kg^{-1} in 1995-1996 to 30-35 µmol kg^{-1} in 2024. C_T and C_{ant} concentrations present positive trends (Table 2, Figure 9a and Supplementary Material Figure S13). No significant changes were observed for A_T (not shown) but we noticed that $\delta^{13}C$ observations in January 2025 were lower than in January 2003 suggesting that surface waters captured the anthropogenic Suess effect signal (Supplementary Material Figure S14) as previously observed in this region (McNeil et al, 2001). Without the BGC-Argo data the C_{ant} trend would be +0.50 ± 0.20 µmol kg^{-}

^{1} yr^{-1}. This is almost the same as derived for surface C_T in winter from the FFNN model (0.44 ±0.01 µmol kg^{-1} yr^{-1}) and equal to the trend derived from only two winter observations (Table 1). The anthropogenic subsurface CO_2 signal was also present in the winter surface data, but these are based on only two observational periods. Our results are similar to previous C_{ant} trend estimates for the region, ranging between +0.35 and +0.65 µmol kg^{-1} yr^{-1} (Pardo et al, 2017). In 2013 low C_{ant} concentrations were estimated in the three layers and were associated with higher temperature, salinity, nitrate and C_T, and lower O_2 concentrations (Supplementary Material Figure S12) probably linked to regional import of warmer Upper Circumpolar Deep Water (UCDW) that contains high C_T, low O_2 and low C_{ant} (e.g. Shadwick et al, 2014; Pardo et al, 2017). The FFNN model produced slightly higher surface C_T concentrations in 2013 (+6 µmol kg^{-1}, Figure 9a, S13d). This 2013 anomaly has very little impact on the estimated trend; removing 2013 yields a trend of +0.42 µmol kg^{-1} yr^{-1} compared to +0.37 µmol kg^{-1} yr^{-1} for the whole time series (Table 2). To quantify the impact of C_{ant} on the C_T, pH_T and Ω_{ar} trends in surface waters, we used both estimates (with or without 2013 data for sensitivity analysis). For the layer 100-150 m, the relationship of C_{ant} versus atmospheric CO_2 concentration, xCO_2 (Figure 9b) are as follow:

All years: $C_{ant} = 0.179 (\pm 0.081) \times xCO_2 - 38.5 (\pm 31.1)$; r2 = 0.41 (Eq. 2)

Without 2013: $C_{ant} = 0.190 (\pm 0.071) \times xCO_2 - 41.6 (\pm 27.2)$; r2 =0.54 (Eq. 3)

Without 2024: $C_{ant} = 0.197 (\pm 0.118) \times xCO_2 - 45.1 (\pm 44.7)$; r2 =0.32 (Eq. 4)

These equations are used to compare the time-series and project the trend in the future.

Table 2: Trends of properties (per year) in layers 100-150m, 150-200m and 200-250m for 1995-2024. Standard-deviations are in bracket. (*) indicates results without the 2013 anomaly. (**) indicates results without the 2013 anomaly and without the 2024 BGC-Argo data.

Layer	T °C.yr^{-1}	Sal yr^{-1}	O_2 µmol kg yr^{-1}	A_T µmol kg yr^{-1}	C_T µmol kg yr^{-1}	C_{ant} µmol kg yr^{-1}
100-150m	-0.018	-0.002	0.37	-0.05	0.29	0.37
	(0.035)	(0.001)	(1.07)	(0.11)	(0.21)	(0.18)
100-150m*	-0.030	-0.002	0.75	-0.05	0.21	0.42
	(0.027)	(0.001)	(0.77)	(0.12)	(0.15)	(0.15)
100-150m**	-0.030	-0.001	1.05	0.10	0.15	0.50
(1995-2018)	(0.039)	(0.001)	(1.08)	(0.14)	(0.21)	(0.20)
150-200m	-0.026	-0.003	0.64	-0.07	0.16	0.37
	(0.038)	(0.001)	(1.21)	(0.12)	(0.24)	(0.23)
200-250m	-0.011	-0.001	0.14	0.03	0.34	0.28
	(0.039)	(0.001)	(1.25)	(0.10)	(0.24)	(0.25)

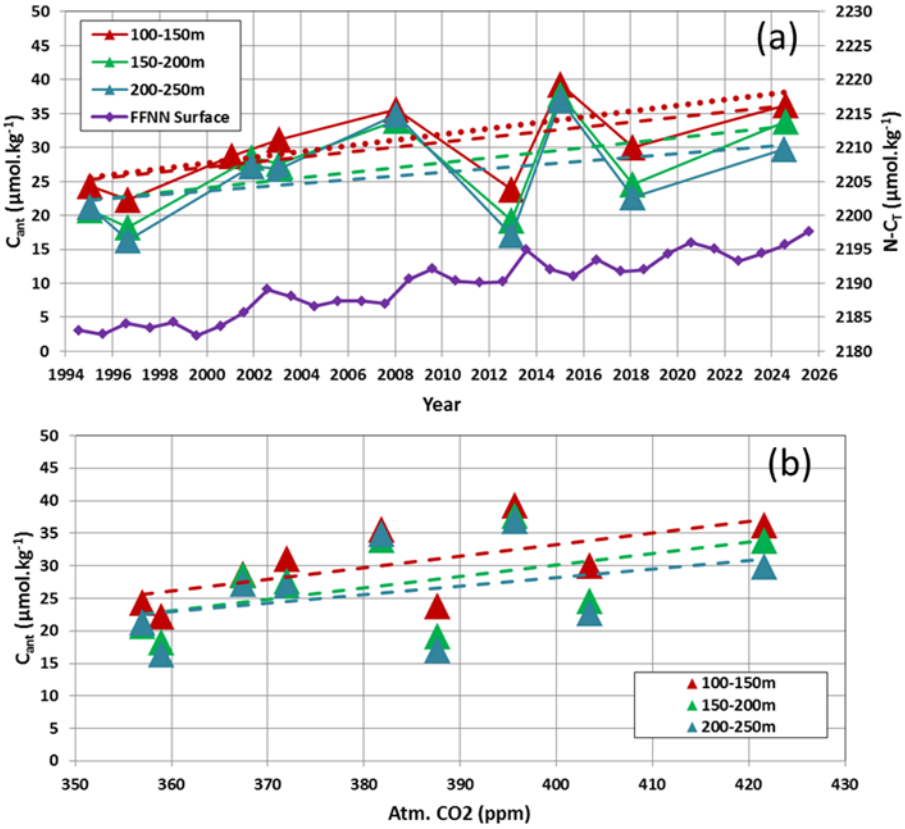


Figure 9: (a): Time-series of anthropogenic CO_2 (C_{ant} µmol kg^{-1}) estimated in 3 layers (below 100m) from 1994 to 2024. The C_{ant} trends are represented by dashed lines (see Table 4). Also shown the N-C_T concentration (µmol.kg^{-1}, right axis) from the FFNN model in August (purple). (b): same data for C_{ant} versus atmospheric CO_2 with associated slopes (dashed lines). For the reconstructed simulation in sea surface waters the results in layer 100-150m were used with (red dashed) or without the 2013 anomaly (red dotted).

3.5 Carbonate system reconstruction and projection in the future

To reconstruct the temporal change of the carbonate system properties (Metzl et al, 2025b) we used the relations between C_{ant} and atmospheric CO_2 described above and calculated the C_T concentration each year correcting C_T as follows, where t represents the time-step in year, from 1960 to 2100:

$$C_T(t) = C_T(t\text{-}1) + C_{ant}(t) - C_{ant}(t\text{-}1) \quad \text{(Eq. 5)}$$

The values of xCO_2 in equation 2, 3 or 4 were derived from SSP emissions scenarios (Shared Socioeconomic Pathways, Meinshausen et al., 2020). We selected a "high" emission scenario SSP5-8.5 and a stabilization scenario SSP2-4.5 and we applied Equation 5 for August using either the C_{ant} trend (Table 2) or Eq. 2 (Eq. 3 or Eq 4 were tested but led to the same results). Temperature, salinity and alkalinity were fixed (SST = -1.8 °C; SSS = 34.2; A_T = 2310 µmol kg^{-1}) and fCO_2, pH_T and Ω_{ar} were calculated using CO2sys_v2.5 (Orr et al, 2018).

The estimated C_T using the C_{ant} trend (Eq. 5) is close to the FFNN model and observations (Figure 10a). The mean difference of C_T between the FFNN model and the C_T estimated for all years

(1985-2025) is -1.72 ±1.53 µmol kg^{-1}. This suggests that anthropogenic CO_2 is a main driver of C_T changes but additional processes need to be included to explain the full trend in surface C_T. In 2009 and 2013 the difference is larger than 4 µmol kg^{-1} (Supplementary Material Figure S15). As discussed above, the import of warm and C_T-rich UCDW in 2013 likely increased the surface C_T. For 2009 there was no data in the water column to explore such scenario but the same process may have occurred.

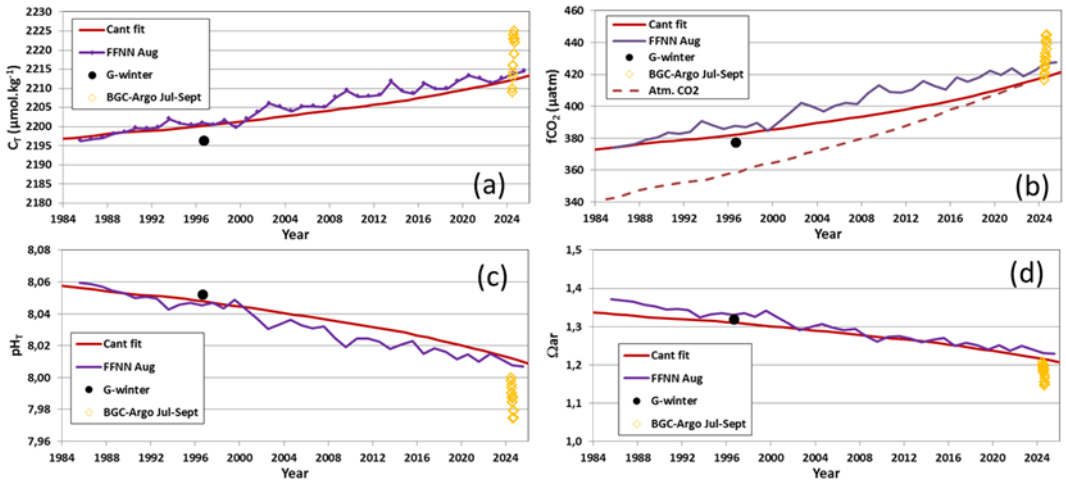


Figure 10: Time-series of (a) C_T concentrations, (b) atmospheric and oceanic fCO_2, (c) pH_T and (d) Ω_{ar} based on a reconstruction for August using C_{ant} fit (red line, see Eq. 2). The reconstruction is compared with the FFNN model (purple), observations in winter 1996 and in winter 2024.

Based on this estimation, we conclude that the anthropogenic CO_2 uptake is responsible for 70% of the C_T increase over 1985-2025. This also drives the decrease of pH_T and Ω_{ar} (Figures 10 c,d). Projecting the trends from the FFNN model and the reconstruction, a value of 1.2 for Ω_{ar} would be reached in year 2032 from the FFNN model against 2034 for the estimation based on Eq. 5. If correct, this would lead to "severe shell dissolution" for pteropods (Bednaršek et al, 2019).

In the Adélie Land region the aragonite saturation depth (ASD, Ω_{ar} = 1) was observed at 1000 m in 1995 and at 700 m in 2011 (Pardo et al, 2017). In summer 2007/2008, Shadwick et al (2014) also reported an ASD around 700-900 m. The data in 2018 and 2024 also identified the ASD at 800-1000 m but Ω_{ar} values close to 1 were also observed at 100m (Figure 11). At around 100-200m depth, this is probably linked to remineralized C_T in the remnant winter water layer, leading to homogeneous and low Ω_{ar} (1.15) after mixing/upwelling in wintertime (Figure 8).

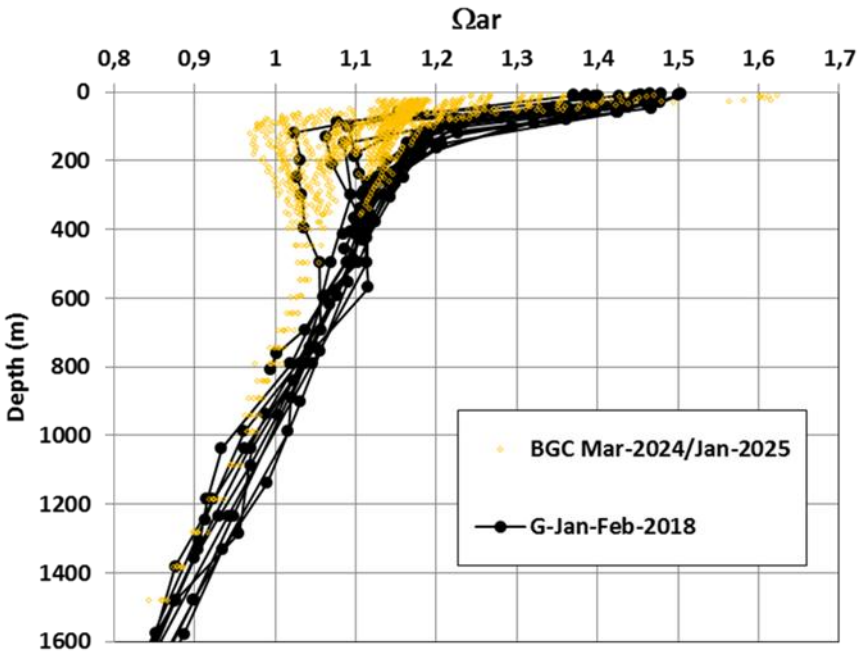


Figure 11: Profiles of Ω_{ar} in Jan-Feb 2018 (GLODAP data, black circles) and in March 2024/January 2025 (BGC-Argo, orange diamonds). Ω_{ar} saturation state (Ω_{ar} =1) occurred at depth (800-1000m) and is also identified around 100m.

We are now interested in exploring when the aragonite undersaturation would be reached in surface waters (Figure 12). The sensitivity analysis based on the two C_{ant}/CO_2 relationships (Eq. 2 and Eq. 3) show similar results. Differences between the two future scenarios (SSP5-8.5 and SSP2-4.5) are large after 2040 (Table 3). For the high scenario, the surface C_T concentrations reaches 2250 µmol kg^{-1} in 2060, a concentration observed in the Adélie Land Bottom Water (ALBW) (Shadwick et al 2014). After 2060, pH_T is lower than 7.9. Based on the high scenario, the aragonite undersaturation would be reached in 2055 (at atmospheric CO_2 = 600 ppm). This is much sooner than deduced in the Southern Ocean from the Coupled Model Intercomparison Project Phase 6 (CMIP6) global models (Ω_{ar} = 1.04 in 2080, Table S9 in Jiang et al, 2023) and would have potential dramatic impact on species such as pteropods (Bednaršek et al, 2012; 2023) as well as for diatoms abundant in the SO (e.g. Petrou et al., 2019; Duncan et al., 2022).

Table 3: Sea surface values of properties in winter for different years and methods in the Adélie Land region (Figure 12). Methods are from observations (Obs.), FFNN model (FFNN) and reconstructions based on two scenarios SSP2-4.5 (SSP45) and SSP2-8.5 (SSP85). For C_{ant} the value is for the layer 100-150m. The last line is for year 2090 using SSP2-85 scenario.

Method	Year	Atm. CO_2	fCO_2	C_T	pH_T	Ω_{ar}	C_{ant}
		ppm	µatm	µmol kg^{-1}	-	-	µmol kg^{-1}
Obs. AT CT	1996	357.6	377.3	2196.3	8.052	1.319	22.3
FFNN	1996	357.6	386.4	2198.3	8.048	1.335	
FFNN	2024	422.8	427.0	2213.9	8.008	1.230	
FFNN	2025	425.7	427.6	2214.5	8.007	1.229	
Obs. BGC	2024	422.8	431.6	2219.4	7.986	1.180	36.3
SSP 85	2024	428.2	417.3	2212.0	8.013	1.218	38.3
SSP 45	2024	426.1	416.1	2211.6	8.014	1.221	37.9
SSP 85	2040	500.0	460.7	2224.8	7.973	1.120	51.2
SSP 45	2040	475.3	445.2	2220.4	7.987	1.153	46.7
SSP 85	2055	600.4	531.6	2242.8	7.916	0.991	69.2
SSP 45	2055	522.3	475.4	2228.8	7.961	1.091	55.2
SSP 85	2060	643.0	565.8	2250.5	7.890	0.938	76.8
SSP 45	2060	537.1	485.4	2231.5	7.952	1.071	57.8
SSP 85	2080	864.4	789.1	2290.2	7.754	0.698	116.5
SSP 45	2080	585.1	520.0	2240.1	7.925	1.010	66.4
SSP 85	2090	998.3	965.7	2314.2	7.670	0.581	140.5

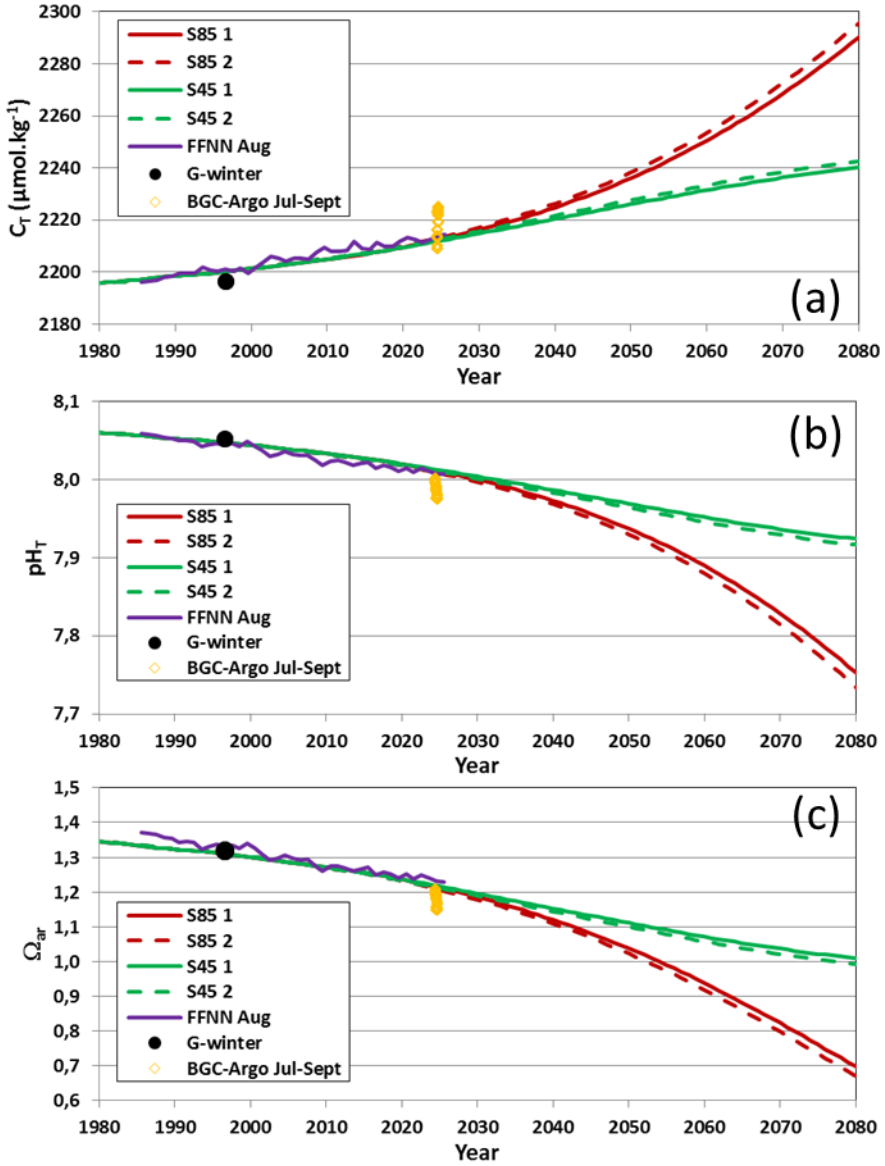


Figure 12: Time-series of (a) C_T concentrations, (b) pH_T and (c) Ωar on a reconstruction for August for two scenarios (SSP85, red line and SSP45 green lines). Observations in winter 1996 and 2024 and the FFNN-LSCE model over 1985-2025 in August (purple) are also shown. The simulations based on C_{ant} trend with (line) or without (dashed) 2013 anomaly are presented.

In our projection, the C_{ant} concentration of 25 µmol kg^{-1} in 1990 will reach 140.5 µmol kg^{-1} in 2090 for the scenario SSP5-8.5. In 2090, a pH_T of 7.67 and an Ω_{ar} of 0.581 are in line with the results of a high-resolution ocean model in the East Antarctica region (a proposed Marine Protected Area, Nissen et al, 2024). Their model suggested that aragonite undersaturation would occur in 2050, coherent with our projection (2055, Figure 12). For a low emission scenario (SSP2-4.5) this would not occur before 2080 (Figure 12).

4. Summary and concluding remarks

New shipboard fCO_2, C_T, A_T and BGC-Argo pH_T observations in 2024 and 2025 and historical fCO_2 data available since 1984 were used to evaluate the decadal trends of the carbonate system in the Adélie Land region.

The sea surface C_T and fCO_2 measurements in summer 2024-2025 present very high variability linked to biological activity. The mean measured fCO_2 observation in January 2025 of 382.3 µatm was much higher than in January 1984 (fCO_2 = 317.5 µatm) but in February 2025 fCO_2 decreased to 317.8 ± 33.8 µatm close to fCO_2 derived from the BGC-Argo float in January 2025 (311.6 ± 12.2 µatm). Previous fCO_2 observations ranged from 179.2 µatm in 2002 to 376.7 µatm in 2007, highlighting the large inter-annual variability in summer.

In summer 2025, the measured C_T between 2130 and 2190 µmol kg^{-1} were much lower than C_T derived from the BGC-Argo data in winter 2024 (2221 µmol kg^{-1}) whereas in winter 1996, the measured C_T was 2207 µmol kg^{-1}. The winter C_T increase from 1996 to 2024 translates into a signal of anthropogenic CO_2 uptake. Using an adapted A_T/S relationship for this region, pH_T and Ω_{ar} were calculated from C_T or fCO_2 data. We estimated a pH_T decrease in surface waters from 8.054 ± 0.005 in winter 1996 (calculated from shipboard data) to 7.976 ± 0.002 in winter 2024 (measured from the BGC-Argo float). The calculated Ω_{ar} decreased from 1.334 ± 0.017 in 1996 to 1.157 ± 0.009 in 2024. Such low Ω_{ar} (1.03 ± 0.10) has been also observed in summer 2015 in the Gerlache Strait, Antarctic Peninsula (Kerr et al, 2018).

As most data were available in summer, the results of a monthly FFNN model were used to estimate the long-term trends. The FFNN model informed that the region was a permanent CO_2 sink and most pronounced since 2006. The maximum sink occurred in 2023 (-1.2 molC m^{-2} yr^{-1}) when the SAM was positive. Results from the FFNN model indicate a pH_T decrease of -0.013 per decade and Ω_{ar} decrease of -0.035 per decade over 1985-2025 in winters. As no change in alkalinity was observed, the OA was mainly explained by the C_T increase (0.44 ±0.01 µmol kg^{-1} yr^{-1}) associated with accumulation of anthropogenic CO_2 calculated from subsurface data since 1995.

A projection of the C_T concentrations in the future, based on observed anthropogenic CO_2 concentrations and emissions scenarios, suggests that aragonite undersaturation would occur in surface water as soon as 2055 with potential impacts on plankton species such as pteropods (and many others species). Interestingly, our data-based analysis is in line with the results of a high-resolution ocean model dedicated to the Marine Protected Areas in the Antarctic coastal zone (Nissen et al, 2024). Their model suggests that climate-change feedbacks, through warming, sea-ice extend, or upwelling, might accelerate OA in these regions. Our simple projection (Figure 12) does not take into account effects of warming, cooling, change of upwelling with C_T-rich waters, or freshening. As opposed to other oceanic regions (Cheng et al, 2025), the Adélie Land coastal region experienced a surface cooling trend of between -0.1 to -0.3°C per decade (Auger et al., 2021, for summer 1993-2017). For the period 1993-2023, Morrow and Kestenare (2025) also estimate a cooling of -0.06 °C per decade and a freshening of -0.012 per decade. Such a cooling and freshening would increase pH_T by only +0.00897 and reduce Ω_{ar} by -0.00112 in 2100 representing a small change compared to the effect of CO_2 emissions. The results presented here support maintaining observations in the Adélie Land region, both from shipboard and BGC-Argo floats, and to investigate property changes and OA in other Antarctic coastal zones.

Competing interests. The contact author has declared that none of the authors has any competing interests.

Acknowledgments:

The Astrolabe data since 1996 were collected as part of a French-Australian collaboration. Underway fCO_2 data from L'Astrolabe 2024-2025 and earlier Australian cruises were sourced from CSIRO and Australia's Integrated Marine Observing System (IMOS) – IMOS is enabled by the National Collaborative Research Infrastructure Strategy (NCRIS). The OISO program on-board Marion-Dufresne was supported by the French institutes INSU (Institut National des Sciences de l'Univers) and IPEV (Institut Polaire Paul-Emile Victor), OSU Ecce-Terra (at Sorbonne Université). We also acknowledge INSU/CNRS and OSU ECCE-Terra for supporting the SNAPO-CO2 facility housed by the LOCEAN laboratory in Paris/France. The development of the neural network model benefited from funding by the French INSU-GMMC project "PPR-Green-Grog (grant no 5-DS-PPR-GGREOG), the EU H2020 project AtlantOS (grant no 633211), as well as through the Copernicus Marine Environment Monitoring Service (project 83-CMEMS-TAC-MOB). MG was funded by the European Union under grant agreement no. 101083922 (OceanICU). Views and opinions expressed are however those of the author(s) only and do not necessarily reflect those of the European Union or European Research Executive Agency. Neither the European Union nor the granting authority can be held responsible for them. The Surface Ocean CO_2 Atlas (SOCAT, www.socat.info) is an international effort, endorsed by the International Ocean Carbon Coordination Project (IOCCP) and the Surface Ocean Lower Atmosphere Study (SOLAS) to deliver a uniformly quality-controlled surface ocean CO_2 database. We thank François Forget, Rafik Hassen-Khodja and Ehouarn Millour for discrete sampling during 2025 L'Astrolabe cruises. Rik Wanninkhof provided comments on a preliminary draft. We thank the associated editor Mathilde Hagens to manage this manuscript, and two anonymous reviewers for their suggestions that helped to improve this article.

Authors contributions:

CLM and NM are co-investigators of the ongoing Océan Indien Service d'Observation (OISO) project. JBS is principal investigator of the Sustained Observation of the Southern Ocean (SOSO) project. BT, JA and CN provided the fCO_2 data, AA analyzed the A_T C_T data and GR provided the C13 data from L'Astrolabe cruises in 2024-2025. NM provided the A_T C_T data from SNAPO-CO2 database. MG and FC developed the CMEMS-LSCE-FFNN model and AB provided the model results. NM started the analysis, wrote the draft of the manuscript and prepared the figures with contributions from all co-authors.

Data availability:

Data used in this study are available in SOCAT (Bakker et al, 2016, www.socat.info) for fCO_2 surface data, and in GLODAP (Lauvset et al, 2023, 2024, www.glodap.info) for water-column data. The A_T and C_T underway data from OISO and MINERVE cruises are available in Seanoe (Metzl et al, 2024a, https://www.seanoe.org, https://doi.org/10.17882/102337). The BGC-Argo float data with derived carbon parameters are available from SOCCOM (https://soccom.org, https://www.mbari.org/products/data-repository/). The CMEMS-LSCE-FFNN model data are available at E.U. Copernicus Marine Service Information (https://resources.marine.copernicus.eu/products, https://doi.org/10.48670/moi-00047).

References

Aoki, S., Y. Kitade, K. Shimada, K. I. Ohshima, T. Tamura, C. C. Bajish, M. Moteki, and S. R. Rintoul: Widespread freshening in the Seasonal Ice Zone near 140E off the Adelie Land Coast, Antarctica, from 1994 to 2012, J. Geophys. Res. Oceans, 118, 6046–6063, doi:10.1002/2013JC009009, 2013.

Arroyo, M. C., Shadwick, E. H., Tilbrook, B., Rintoul, S. R., and Kusahara, K.: A continental shelf pump for CO2 on the Adélie Land coast, East Antarctica. Journal of Geophysical Research: Oceans, 125, e2020JC016302. https://doi.org/10.1029/2020JC016302, 2020.

Auger, M., Morrow, R., Kestenare, E., Sallée, J.-B., and Cowley, R.: Southern Ocean in-situ temperature trends over 25 years emerge from interannual variability, Nat. Commun., 12, 514, https://doi.org/10.1038/s41467-020-20781-1, 2021.

Bakker, D. C. E., Pfeil, B., Landa, C. S., Metzl, N., O'Brien, K. M., Olsen, A., Smith, K., Cosca, C., Harasawa, S., Jones, S. D., Nakaoka, S.-I., Nojiri, Y., Schuster, U., Steinhoff, T., Sweeney, C., Takahashi, T., Tilbrook, B., Wada, C., Wanninkhof, R., Alin, S. R., Balestrini, C. F., Barbero, L., Bates, N. R., Bianchi, A. A., Bonou, F., Boutin, J., Bozec, Y., Burger, E. F., Cai, W.-J., Castle, R. D., Chen, L., Chierici, M., Currie, K., Evans, W., Featherstone, C., Feely, R. A., Fransson, A., Goyet, C., Greenwood, N., Gregor, L., Hankin, S., Hardman-Mountford, N. J., Harlay, J., Hauck, J., Hoppema, M., Humphreys, M. P., Hunt, C. W., Huss, B., Ibánhez, J. S. P., Johannessen, T., Keeling, R., Kitidis, V., Körtzinger, A., Kozyr, A., Krasakopoulou, E., Kuwata, A., Landschützer, P., Lauvset, S. K., Lefèvre, N., Lo Monaco, C., Manke, A., Mathis, J. T., Merlivat, L., Millero, F. J., Monteiro, P. M. S., Munro, D. R., Murata, A., Newberger, T., Omar, A. M., Ono, T., Paterson, K., Pearce, D., Pierrot, D., Robbins, L. L., Saito, S., Salisbury, J., Schlitzer, R., Schneider, B., Schweitzer, R., Sieger, R., Skjelvan, I., Sullivan, K. F., Sutherland, S. C., Sutton, A. J., Tadokoro, K., Telszewski, M., Tuma, M., Van Heuven, S. M. A. C., Vandemark, D., Ward, B., Watson, A. J., Xu, S.: A multi-decade record of high-quality fCO_2 data in version 3 of the Surface Ocean CO_2 Atlas (SOCAT), Earth Syst. Sci. Data, 8, 383-413, doi:10.5194/essd-8-383-2016. 2016.

Bakker, Dorothee C. E.; Alin, Simone R.; Aramaki, Takafumi; Barbero, Leticia; Bates, Nicholas; Gkritzalis, Thanos; Jones, Steve D.; Kozyr, Alex; Lauvset, Siv K.; Macovei, Vlad A.; Metzl, Nicolas; Munro, David R.; Nakaoka, Shin-ichiro; O'Brien, Kevin M.; Olsen, Are; Pierrot, Denis; Steinhoff, Tobias; Sullivan, Kevin F.; Sutton, Adrienne J.; Sweeney, Colm; Wada, Chisato; Wanninkhof, Rik; Akl, John; Arbilla, Lisandro A.; Azetsu-Scott, Kumiko; Battisti, Roman; Beatty, Cory M.; Becker, Meike; Benoit-Cattin, Alice; Berghoff, Carla F.; Bittig, Henry C.; Bonin, Jennifer A.; Bott, Randy; Bozzano, Roberto; Burger, Eugene F.; Brunetti, Fabio; Cantoni, Carolina; Castelli, Giuliano; Chambers, Don P.; Chierici, Melissa; Corbo, Andrea; Cronin, Margot; Cross, Jessica N.; Currie, Kim I.; Dentico, Carlotta; Emerson, Steven R.; Enochs, Ian C.; Enright, Matt P.; Enyo, Kazutaka; Ericson, Ylva; Evans, Wiley; Fay, Amanda R.; Feely, Richard A.; Fragiacomo, Elena; Fransson, Agneta; Gehrung, Martina; Giani, Michele; Glockzin, Michael; Hamnca, Siyabulela; Holodkov, Nikola; Hoppema, Mario; Ibánhez, J. Severino P.; Kadono, Koji; Kamb, Linus; Kralj, Martina; Kristensin, Tor O.; Laudicella, V. Alessandro; Lefèvre, Nathalie; Leseurre, Coraline; Lo Monaco, Claire; Maenner Jones, Stacy; Maenza, Reinaldo A.; McAuliffe, Anna M.; Mdokwana, Baxolele; Monacci, Natalie M.; Musielewicz, Sylvia; Neill, Craig; Newberger, Tim; Nojiri, Yukihiro; Ohman, Mark D.; Ólafsdóttir, Sólveig R.; Olivier, Léa; Omar, Abdirahman M.; Osborne, John; Pensieri, Sara; Petersen, Wilhelm; Plueddemann, Albert J.; Rehder, Gregor; Roden, Nicholas P.; Rutgersson, Anna; Sallée, Jean-Baptiste; Sanders, Richard; Sarpe, Dick; Schirnik, Carsten; Schlitzer, Reiner; Send, Uwe; Skjelvan, Ingunn; Sutherland, Stewart, C.; T'Jampens,

Michiel; Tamsitt, Veronica; Telszewski, Maciej; Theetaert, Hannelore; Tilbrook, Bronte; Trull, Tom; Tsanwani, Mutshutshu; Van de Velde, Sebastiaan; Van Heuven, Steven M. A. C.; Veccia, Martín H.; Voynova, Yoana G.; Weller, Robert A.; Williams, Nancy L.: Surface Ocean CO2 Atlas Database Version 2025 (SOCATv2025) (NCEI Accession 0304549). [indicate subset used]. NOAA National Centers for Environmental Information. Dataset. https://doi.org/10.25921/648f-fv35. Last Access 5 June 2025, 2025.

Barrett, R. C., Carter, B. R., Fassbender, A. J., Tilbrook, B., Woosley, R. J., Azetsu-Scott, K., R. A. Feely, C. Goyet, M. Ishii, A. Murata and F. Pérez: Biological responses to ocean acidification are changing the global ocean carbon cycle. Global Biogeochemical Cycles, 39, e2024GB008358. https://doi.org/10.1029/2024GB008358, 2025.

Bednaršek, N. , G. A. Tarling, D. C. E. Bakker, S. Fielding, E. M. Jones, H. J. Venables, P.Ward, A. Kuzirian, B. Lézé, R. A. Feely and E. J. Murphy: Extensive dissolution of live pteropods in the Southern Ocean. Nat. Geosci. 5, 881–885, DOI: 10.1038/NGEO1635, 2012.

Bednaršek N, Feely R. A., Howes E. L., Hunt B. P. V., Kessouri F., León P., Lischka S., Maas A. E., McLaughlin K., Nezlin N. P., Sutula M. and Weisberg S. B.: Systematic Review and Meta-Analysis Toward Synthesis of Thresholds of Ocean Acidification Impacts on Calcifying Pteropods and Interactions With Warming. Front. Mar. Sci. 6:227. doi: 10.3389/fmars.2019.00227, 2019.

Bednaršek, N., R. A. Feely, G. Pelletier, and F. Desmet: Global synthesis of the status and trends of ocean acidification impacts on shelled pteropods. Oceanography 36(2–3):130–137, https://doi.org/10.5670/oceanog.2023.210, 2023.

Bender, M. L., Tilbrook, B., Cassar, N., Jonsson, B., Poisson, A., and Trull, T. W.: Ocean productivity south of Australia during spring and summer, Deep Sea Research Part I: Oceanographic Research Papers, Volume 112, Pages 68-78, https://doi.org/10.1016/j.dsr.2016.02.018, 2016.

Beucher, C., P. Tréguer, A.-M. Hapette, R. Corvaisier, N. Metzl, and J.-J. Pichon: Intense summer Si-recycling in the surface Southern Ocean, Geophys. Res. Lett., 31, L09305, doi:10.1029/2003GL018998, 2004.

Boothroyd, A., Adams, V., Alexander, K., and Hill, N.: Stakeholder perceptions of the Commission for the Conservation of Antarctic Marine Living Resources Marine Protected Area planning process. Marine Policy, 170, Article 106381. https://doi.org/10.1016/j.marpol.2024.106381, 2024.

Bourgeois, T., J. C. Orr, L. Resplandy, J. Terhaar, C. Ethé, M. Gehlen, and L. Bopp: Coastal-ocean uptake of anthropogenic carbon. Biogeosciences, 13, 4167-4185, doi: 10.5194/bg-13-4167-2016., 2016.

Brandon, M., Goyet, C., Touratier, F., Lefèvre, N., Kestenare, E., and Morrow, R.: Spatial and temporal variability of the physical, carbonate and CO2 properties in the Southern Ocean surface waters during austral summer (2005-2019), *Deep-Sea Research Part I*, https://doi.org/10.1016/j.dsr.2022.103836, 2022.

Brévière, E., N.Metzl, A.Poisson and B.Tilbrook: Changes of oceanic CO2 sink in the Eastern Indian sector of the Southern Ocean. Tellus, 58B, 438-446, 10.1111/j.1600-0889.2006.00220.x, 2006.

Carter, B. R., Williams, N. L., Gray, A. R., and Feely, R. A.: Locally interpolated alkalinity regression for global alkalinity estimation. Limnol. Oceanogr.: Methods 14: 268–277. doi:10.1002/lom3.10087, 2016.

Carter, B. R., Feely, R. A., Williams, N. L., Dickson, A. G., Fong, M. B., and Takeshita, Y.: Updated methods for global locally interpolated estimation of alkalinity, pH, and nitrate. Limnology and Oceanography: Methods, 16: 119-131. doi: 10.1002/lom3.10232, 2017.

Carter, B.R., Feely, R.A., Wanninkhof, R., Kouketsu, S., Sonnerup, R.E., Pardo, P.C., Sabine, C.L., Johnson, G.C., Sloyan, B.M., Murata, A., Mecking, S., Tilbrook, B., Speer, K., Talley, L.D., Millero, F.J., Wijffels, S.E., Macdonald, A.M., Gruber, N., Bullister, J.L.: Pacific anthropogenic carbon between 1991 and 2017. Global Biogeochem. Cycles 33, 597–617. https://doi.org/10.1029/2018GB006154, 2019.

Chau, T. T. T., Gehlen, M., and Chevallier, F.: A seamless ensemble-based reconstruction of surface ocean pCO2 and air–sea CO2 fluxes over the global coastal and open oceans, Biogeosciences, 19, 1087–1109, https://doi.org/10.5194/bg-19-1087-2022, 2022.

Chau, T.-T.-T., Gehlen, M., Metzl, N., and Chevallier, F.: CMEMS-LSCE: a global, 0.25°, monthly reconstruction of the surface ocean carbonate system, Earth Syst. Sci. Data, 16, 121–160, https://doi.org/10.5194/essd-16-121-2024, 2024a.

Chau, T.-T.-T., Chevallier, F., and Gehlen, M.. Global analysis of surface ocean CO2 fugacity and air-sea fluxes with low latency. Geophysical Research Letters, 51, e2023GL106670. https://doi. org/10.1029/2023GL106670, 2024b.

Cheng, L., Abraham, J., Trenberth, K. E., Reagan, J., Zhang, H.-M., Storto, A., Von Schuckmann, K., Pan, Y., Zhu, Y., Mann, M. E., Zhu, J., Wang, F., Yu, F., Locarnini, R., Fasullo, J., Huang, B., Graham, G., Yin, X., Gouretski, V., Zheng, F., Li, Y., Zhang, B., Wan, L., Chen, X., Wang, D., Feng, L., Song, X., Liu, Y., Reseghetti, F., Simoncelli, S., Chen, G., Zhang, R., Mishonov, A., Tan, Z., Wei, W., Yuan, H., Li, G., Ren, Q., Cao, L., Lu, Y., Du, J., Lyu, K., Sulaiman, A., Mayer, M., Wang, H., Ma, Z., Bao, S., Yan, H., Liu, Z., Yang, C., Liu, X., Hausfather, Z., Szekely, T., and Gues, F.: Record High Temperatures in the Ocean in 2024, Adv. Atmos. Sci., 42, 1092–1109, https://doi.org/10.1007/s00376-025-4541-3, 2025.

Deng, P., He, S., Zhang, Z., Smith, W. O., Jr., He, J., Lan, M., Du, Z. , and Le, C.: Increased carbon sink within the seasonal sea ice zone associated with climate variability in the Southern Ocean. Geophysical Research Letters, 52, e2025GL118274. https://doi.org/10.1029/2025GL118274, 2025.

Dickson, A. G. : Standard potential of the reaction: AgCl(s) + ½H2(g) = Ag(s) + HCl(aq), and the standard acidity constant of the ion HSO4– in synthetic sea water from 273.15 to 318.15 K. J. Chem. Thermodyn. 22: 113–127. doi:10.1016/0021-9614(90)90074-Z, 1990.

Dickson, A. G., Sabine, C. L., and Christian, J. R.: Guide to best practices for ocean CO2 measurements, North Pacific Marine Science Organization, Sidney, British Columbia, 191, https://doi.org/10.25607/OBP-1342, 2007.

Duncan, R. J., Nielsen, D. A., Sheehan, C. E., Deppeler, S., Hancock, A. M., Schulz, K. G., Davidson, A. T. and Petrou, K.: Ocean acidification alters the nutritional value of Antarctic diatoms. New Phytol, 233: 1813-1827. https://doi-org.insu.bib.cnrs.fr/10.1111/nph.17868, 2022.

Edmond, J. M.: High precision determination of titration alkalinity and total carbon dioxide content of sea water by potentiometric titration. Deep-Sea Res. 17, 737–750. https://doi.org/10.1016/0011-7471(70)90038-0., 1970.

Fay, A. R., Munro, D. R., McKinley, G. A., Pierrot, D., Sutherland, S. C., Sweeney, C., and Wanninkhof, R.: Updated climatological mean ΔfCO2 and net sea–air CO2 flux over the global open ocean regions, Earth Syst. Sci. Data, 16, 2123–2139, https://doi.org/10.5194/essd-16-2123-2024, 2024.

Garcia, H. E., Weathers, K. W., Paver, C. R., Smolyar, I., Boyer, T. P., Locarnini, R. A., Zweng, M. M., Mishonov, A. V., Baranova, O. K., Seidov, D., and Reagan, J. R.: World Ocean Atlas 2018. Vol. 4: Dissolved Inorganic Nutrients (phosphate, nitrate and nitrate+nitrite, silicate). A. Mishonov Technical Editor, NOAA Atlas NESDIS 84, 35 pp., https://archimer.ifremer.fr/doc/00651/76336/ (last access: 30 July 2022), 2019.

Gordon, A. L., and Tchernia, P. L.: Waters of the continental margin off Adelie Coast, Antarctica. Antarctica Oceanology II: The Australian-New Zealand Sector, 59-69, 1972.

Gkritzalis, T., D. C. E. Bakker, S. K. Lauvset, and T. Steinhoff: SOCAT Quality Control Cookbook - For version 2025 of the Surface Ocean CO2 Atlas. Available at www.socat.info, last access, 29-June-2026., 2024.

Hauck J., Hoppema, M., Bellerby, R. G. J., Völker, C., and Wolf-Gladrow, D.: Data-based estimation of anthropogenic carbon and acidification in the Weddell Sea on a decadal timescale. J. Geophys. Res. 115, C03004. doi:10.1029/2009jc005479, 2010.

Ishii, M., Inoue, H. Y., and Matsueda, H.: Net community production in the marginal ice zone and its importance for the variability of the oceanic pCO2 in the Southern Ocean south of Australia. Deep Sea Research Part II: Topical Studies in Oceanography, 49(9), 1691–1706. https://doi.org/10.1016/s0967-0645(02)00007-3, 2002.

Jiang, L.-Q., Dunne, J., Carter, B. R., Tjiputra, J. F., Terhaar, J., Sharp, J. D., Olsen, A., Alin, S., Bakker, D. C. E., Feely, R. A., Gattuso, J.-P., Hogan, P., Ilyina, T., Lange, N., Lauvset, S. K., Lewis, E. R., Lovato, T., Palmieri, J., Santana-Falcón, Y., Schwinger, J., Séférian, R., Strand, G., Swart, N., Tanhua, T., Tsujino, H., Wanninkhof, R., Watanabe, M., Yamamoto, A., and Ziehn, T.: Global surface ocean acidification indicators from 1750 to 2100, J. Adv. Model. Earth Sy., 15, e2022MS003563, https://doi.org/10.1029/2022MS003563, 2023.

Kerr, R., C. Goyet, L. C. da Cunha, I. B. M. Orselli, J. M. Lencina-Avila, C. R. B. Mendes, M. Carvalho-Borges, M. M. Mata, and V. M. Tavano : Carbonate system properties in the Gerlache Strait, Northern Antarctic Peninsula (February 2015): II. Anthropogenic CO2 and seawater acidification. Deep. Res. Part II. 149, 182–192. https://doi.org/10.1016/j.dsr2.2017.07.007, 2018.

Laika, H. E., Goyet C., Vouve F., Poisson A., and Touratier F.: Interannual properties of the CO2 system in the Southern Ocean south of Australia. Antarctic Science, 21(6), 663-680. https://doi.org/10.1017/S0954102009990319, 2009.

Landschützer, P., Gruber, N., Bakker, D. C. E., Stemmler, I., and Six, K. D.: Strengthening seasonal marine CO2 variations due to increasing atmospheric CO2. Nature Climate Change, 8(2), 146–150. https://doi.org/10.1038/s41558-017-0057-x, 2018.

Laruelle, G. G., Cai, W.-J., Hu, X., Gruber, N., Mackenzie, F. T., and Regnier, P.: Continental shelves as a variable but increasing global sink for atmospheric carbon dioxide. Nat.Commun. 9, 454, DOI: 10.1038/s41467-017-02738-z, 2018.

Lauvset, S. K., Lange, N., Tanhua, T., Bittig, H. C., Olsen, A., Kozyr, A., Álvarez, M., Azetsu-Scott, K., Brown, P. J., Carter, B. R., Cotrim da Cunha, L., Hoppema, M., Humphreys, M. P., Ishii, M., Jeansson, E., Murata, A., Müller, J. D., Pérez, F. F., Schirnick, C., Steinfeldt, R., Suzuki, T., Ulfsbo, A., Velo, A., Woosley, R. J., and Key, R. M.: The annual update GLODAPv2.2023: the global interior ocean biogeochemical data product, Earth Syst. Sci. Data, 16, 2047–2072, https://doi.org/10.5194/essd-16-2047-2024, 2024.

Lauvset, Siv K.; Lange, Nico; Tanhua, Toste; Bittig, Henry C.; Olsen, Are; Kozyr, Alex; Álvarez, Marta; Azetsu-Scott, Kumiko; Becker, Susan; Brown, Peter J.; Carter, Brendan R.; Cotrim da Cunha, Leticia; Feely, Richard A.; Hoppema, Mario; Humphreys, Matthew P.; Ishii, Masao; Jeansson, Emil; Jones, Steve D.; Lo Monaco, Claire; Murata, Akihiko; Müller, Jens Daniel; Pérez, Fiz F.; Schirnick, Carsten; Steinfeldt, Reiner; Suzuki, Toru; Tilbrook, Bronte; Ulfsbo, Adam; Velo, Antón; Woosley, Ryan J.; Key, Robert M.: Global Ocean Data Analysis Project version 2.2023 (GLODAPv2.2023) (NCEI Accession 0283442). [indicate subset used]. NOAA National Centers for Environmental Information. Dataset. https://doi.org/10.25921/zyrq-ht66. Last Access [4 June 2025], 2023?

Lee, K., Tong, L. T., Millero, F. J., Sabine, C. L., Dickson, A. G., Goyet, C., Park, G. H., Wanninkhof, R., Feely, R. A., and Key, R. M.: Global relationships of total alkalinity with salinity and temperature in surface waters of the world's oceans. Geophys. Res. Lett. 33, L19605. doi10.1029/2006GL027207, 2006.

Leseurre, C., Lo Monaco, C., Reverdin, G., Metzl, N., Fin, J., Mignon, C., and Benito, L.: Summer trends and drivers of sea surface fCO2 and pH changes observed in the southern Indian Ocean over the last two decades (1998–2019), Biogeosciences, 19, 2599–2625, https://doi.org/10.5194/bg-19-2599-2022, 2022.

Lueker, T.J., Dickson, A.G., Keeling, C.D.: Ocean pCO(2) calculated from dissolved inorganic carbon, alkalinity, and equations for K-1 and K-2: validation based on laboratory measurements of CO2 in gas

and seawater at equilibrium. Marine Chemistry 70, 105-119. https://doi.org/10.1016/S0304-4203(00)00022-0, 2000.

Mahieu, L., Lo Monaco, C., Metzl, N., Fin, J., and Mignon, C.: Variability and stability of anthropogenic CO_2 in Antarctic Bottom Water observed in the Indian sector of the Southern Ocean, 1978–2018, Ocean Sci., 16, 1559–1576, https://doi.org/10.5194/os-16-1559-2020, 2020.

Marshall, G. J.: Trends in the Southern Annular Mode from observations and reanalyses. J. Clim., 16, 4134-4143, doi:10.1175/1520-0442%282003%29016<4134%3ATITSAM>2.0.CO%3B2, 2003.

Mazloff, M. R., Verdy, A., Gille, S. T., Johnson, K. S., Cornuelle, B. D., and Sarmiento, J.: Southern Ocean acidification revealed by biogeochemical-Argo floats. Journal of Geophysical Research: Oceans, 128, e2022JC019530. https://doi.org/10.1029/2022JC019530, 2023.

McNeil, B. I., Tilbrook, B. and Matear, R. J.: Accumulation and uptake of anthropogenic CO2 in the Southern Ocean, south of Australia between 1968 and 1996, J. Geophys. Res., 106, C12, 31431-31445, doi:10.1029/2000JC000331, 2001.

Meinshausen, M., Nicholls, Z. R. J., Lewis, J., Gidden, M. J., Vogel, E., Freund, M., Beyerle, U., Gessner, C., Nauels, A., Bauer, N., Canadell, J. G., Daniel, J. S., John, A., Krummel, P. B., Luderer, G., Meinshausen, N., Montzka, S. A., Rayner, P. J., Reimann, S., Smith, S. J., van den Berg, M., Velders, G. J. M., Vollmer, M. K., and Wang, R. H. J.: The shared socioeconomic pathway (SSP) greenhouse gas concentrations and their extensions to 2500, Geosci. Model Dev., 13, 3571–3605, https://doi.org/10.5194/gmd-13-3571-2020, 2020.

Metzl, N., B.Tilbrook and A. Poisson: The annual fCO2 cycle and the air-sea CO2 flux in the sub-Antarctic Ocean. Tellus, 51B, 4, 849-861. https://doi.org/10.1034/j.1600-0889.1999.t01-3-00008.x, 1999.

Metzl Nicolas, Fin Jonathan, Lo Monaco Claire, Mignon Claude, Alliouane Samir, Bombled Bruno, Boutin Jacqueline, Bozec Yann, Comeau Steeve, Conan Pascal, Coppola Laurent, Cuet Pascale, Ferreira Eva, Gattuso Jean-Pierre, Gazeau Frédéric, Goyet Catherine, Grossteffan Emilie, Lansard Bruno, Lefèvre Dominique, Lefèvre Nathalie, Leseurre Coraline, Lombard Fabien, Petton Sébastien, Pujo-Pay Mireille, Rabouille Christophe, Reverdin Gilles, Ridame Céline, Rimmelin-Maury Peggy, Ternon Jean-François, Touratier Franck, Tribollet Aline, Wagener Thibaut, Wimart-Rousseau Cathy: An updated synthesis of ocean total alkalinity and dissolved inorganic carbon measurements from 1993 to 2023: the SNAPO-CO2-v2 dataset. SEANOE. https://doi.org/10.17882/102337, 2024a.

Metzl, N., Lo Monaco, C., Leseurre, C., Ridame, C., Reverdin, G., Chau, T. T. T., Chevallier, F., and Gehlen, M.: Anthropogenic CO2, air–sea CO2 fluxes, and acidification in the Southern Ocean: results from a time-series analysis at station OISO-KERFIX (51° S–68° E), Ocean Sci., 20, 725–758, https://doi.org/10.5194/os-20-725-2024, 2024b.

Metzl, N., Fin, J., Lo Monaco, C., Mignon, C., Alliouane, S., Bombled, B., Boutin, J., Bozec, Y., Comeau, S., Conan, P., Coppola, L., Cuet, P., Ferreira, E., Gattuso, J.-P., Gazeau, F., Goyet, C., Grossteffan, E.,

Lansard, B., Lefèvre, D., Lefèvre, N., Leseurre, C., Petton, S., Pujo-Pay, M., Rabouille, C., Reverdin, G., Ridame, C., Rimmelin-Maury, P., Ternon, J.-F., Touratier, F., Tribollet, A., Wagener, T., and Wimart-Rousseau, C.: An updated synthesis of ocean total alkalinity and dissolved inorganic carbon measurements from 1993 to 2023: the SNAPO-CO2-v2 dataset, Earth Syst. Sci. Data, 17, 1075–1100, https://doi.org/10.5194/essd-17-1075-2025, 2025a.

Metzl, N., Lo Monaco, C., Tribollet, A., Ternon, J.-F., Chevallier, F., and Gehlen, M.: New observations confirm the progressive acidification in the Mozambique Channel, Biogeosciences, 22, 7187–7204, https://doi.org/10.5194/bg-22-7187-2025, 2025b.

Midorikawa, T., Inoue, H. Y., Ishii, M., Sasano, D., Kosugi, N., Hashida, G., Nakaoka, S., and Suzuki, T.: Decreasing pH trend estimated from 35-year time series of carbonate parameters in the Pacific sector of the Southern Ocean in summer, Deep-Sea Res., 61, 131–139, https://doi.org/10.1016/j.dsr.2011.12.003, 2012.

Millero, F. J., Lee, K., Roche, M.: Distribution of alkalinity in the surface waters of the major oceans. Mar. Chem. 60, 111–130. https://doi.org/10.1016/S0304-4203(97)00084-4, 1998

Monteiro, T., Kerr, R., Orselli, I.B.M., Lencina-Avila, J.M.: Towards an intensified summer CO2 sink behaviour in the Southern Ocean coastal regions, Progress in Oceanography, doi: https://doi.org/10.1016/j.pocean.2020.102267, 2020.

Morrow, R. and Kestenare, E.: 30 years of sea surface temperature and salinity observations crossing the Southern Ocean near 140°E: Trends and rollercoaster variability, Journal of Marine System, https://doi.org/10.1016/j.jmarsys.2025.104048, 2025.

Munro, D. R., N. S. Lovenduski, T. Takahashi, B. B. Stephens, T. Newberger, and C. Sweeney: Recent evidence for a strengthening CO2 sink in the Southern Ocean from carbonate system measurements in the Drake Passage (2002–2015), Geophys. Res. Lett., 42, doi:10.1002/2015GL065194, 2015.

Nissen, C., Lovenduski, N. S., Brooks, C. M., Hoppema, M., Timmermann, R., and Hauck, J.: Severe 21st-century ocean acidification in Antarctic Marine Protected Areas. Nat. Commun., 15, 259. https://doi.org/10.1038/s41467-023-44438-x, 2024.

Orr, J. C., Epitalon, J.-M., Dickson, A. G., and Gattuso, J.-P.: Routine uncertainty propagation for the marine carbon dioxide system, Marine Chemistry, Vol. 207, 84-107, doi:10.1016/j.marchem.2018.10.006., 2018.

Petrou, K., Baker, K. G., Nielsen, D. A., Hancock, A. M., Schulz, K. G. and Davidson, A. T.: Acidification diminishes diatom silica production in the Southern Ocean. Nature Climate Change, 9, 781-786, https://doi.org/10.1038/s41558-019-0557-y, 2019.

Pardo, P. C., Tilbrook, B., Langlais, C., Trull, T. W., and Rintoul, S. R.: Carbon uptake and biogeochemical change in the Southern Ocean, south of Tasmania. Biogeosciences, 14(22), 5217–5237. https://doi.org/10.5194/bg-14-5217-2017, 2017.

Pierrot, D., C. Neill, K. Sullivan, R. Castle, R. Wanninkhof, H. Lüger, T. Johannessen, A. Olsen, R. A. Feely, C. E. Cosca: Recommendations for Autonomous Underway pCO2 Measuring Systems and Data Reduction Routines, Deep-Sea Research II, doi:10.1016/j.dsr2.2008.12.005, 2009.

Rodgers, K. B., Schwinger, J., Fassbender, A. J., Landschützer, P., Yamaguchi, R., Frenzel, H., Stein, K., Müller, J. D., Goris, N., Sharma, S., Bushinsky, S., Chau, T. T. T., Gehlen, M., Gallego, M. A., Gloege, L., Gregor, L., Gruber, N., Hauck, J., Iida, Y., Ishii, M., Keppler, L., Kim, J. E., Schlunegger, S., Tjiputra, J., Toyama, K., Ayar, P. V., and Velo, A.: Seasonal variability of the surface ocean carbon cycle: A synthesis, Global Biogeochem. Cy., 37, e2023GB007798, https://doi.org/10.1029/2023GB007798, 2023.

Roobaert, A., Resplandy, L., Laruelle, G. G., Liao, E., and Regnier, P.: Unraveling the physical and biological controls of the global coastal CO2 sink. Global Biogeochemical Cycles, 38, e2023GB007799. https://doi.org/10.1029/2023GB007799, 2024a.

Roobaert, A., Regnier, P., Landschützer, P., and Laruelle, G. G.: A novel sea surface pCO2-product for the global coastal ocean resolving trends over 1982–2020, Earth Syst. Sci. Data, 16, 421–441, https://doi.org/10.5194/essd-16-421-2024, 2024b.

Shadwick, E., Rintoul, S., Tilbrook, B., Williams, G., Young, N., Fraser, A. D., Marchant, H., Smith, J., and Tamura, T.: Glacier tongue calving reduced dense water formation and enhanced carbon uptake. Geophysical Research Letters, 40(5), 904–909. https://doi.org/10.1002/grl.50178, 2013.

Shadwick, E. H., B. Tilbrook, and G. D. Williams: Carbonate chemistry in the Mertz Polynya (East Antarctica): Biological and physical modification of dense water outflows and the export of anthropogenic CO2, J. Geophys. Res. Oceans, 119, 1–14, doi:10.1002/2013JC009286, 2014.

Shadwick, E. H., B. Tilbrook, and K. I. Currie: Late-summer biogeochemistry in the Mertz Polynya: East Antarctica, J. Geophys. Res. Oceans, 122, 7380–7394, doi:10.1002/2017JC013015, 2017.

Shadwick, E. H., Wynn-Edwards, C. A., Matear, R.J., Jansen, P., Schulz, E. and Sutton, A. J.: Observed amplification of the seasonal CO2 cycle at the Southern Ocean Time Series. Front. Mar. Sci. 10:1281854. doi: 10.3389/fmars.2023.1281854, 2023.

Schlitzer, R.: Ocean Data View, http:/odv.awi.de, 2018.

Sholeninova, P., Morrison, A. K., McC. Hogg, A., and Foppert, A.: Quantification of Antarctic bottom water pathways in the Australian-Antarctic Basin. Journal of Geophysical Research: Oceans, 130, e2024JC022305. https://doi.org/10.1029/2024JC022305, 2025.

Stark, J. S., N. P. Roden, G. J. Johnstone, M. Milnes, J. G. Black, S. Whiteside, W. Kirkwood, K. Newbery, S. Stark, E. van Ooijen, B. Tilbrook, E. T. Peltzer, K. Berry and D. Roberts: Carbonate chemistry of an in-situ free-ocean CO2 enrichment experiment (antFOCE) in comparison to short

term variation in Antarctic coastal waters. Scientific ReportS, 8:2816, DOI:10.1038/s41598-018-21029-1., 2018.

Takahashi, T., Olafsson, J., Goddard, J. G., Chipman, D. W., and Sutherland, S. C.: Seasonal variation of CO2 and nutrients in the high-latitude surface oceans: A comparative study, Global Biogeochem. Cycles, 7, 843–878, https://doi.org/10.1029/93GB02263, 1993.

Takahashi, T., Sutherland, S. C., Wanninkhof, R., Sweeney, C., Feely, R. A., Chipman, D. W., Hales, B., Friederich, G., Chavez, F., Sabine, C., Watson, A., Bakker, D. C., Schuster, U., Metzl, N., Yoshikawa-Inoue, H., Ishii, M., Midorikawa, T., Nojiri, Y., Körtzinger, A., Steinhoff, T., Hoppema, M., Olafsson, J., Arnarson, T. S., Tilbrook, B., Johannessen, T., Olsen, A., Bellerby, R., Wong, C., Delille, B., Bates, N., and de Baar, H. J.: Climatological mean and decadal change in surface ocean pCO2, and net sea–air CO2 flux over the global oceans, Deep-Sea Res. Pt. II, 56, 554–577, https://doi.org/10.1016/j.dsr2.2008.12.009, 2009.

Takahashi, T., Sutherland, S.C., Chipman, D.W., Goddard, J.G., Ho, C., Newberger, T., Sweeney, C., Munro, D.R.: Climatological distributions of pH, pCO2, total CO2, alkalinity, and CaCO3 saturation in the global surface ocean, and temporal changes at selected locations. Mar. Chem. 164, 95–125. https://doi.org/10.1016/j.marchem.2014.06.004, 2014.

Tilbrook, B., E. B. Jewett , M. D. DeGrandpre, J. M. Hernandez-Ayon, , R. A. Feely, D. K. Gledhill, L. Hansson, K. Isensee, M. L. Kurz, J. A. Newton, S. A. Siedlecki, F. Chai, S. Dupont, M. Graco, E. Calvo, D. Greeley, L. Kapsenberg, M. Lebrec, C. Pelejero, K. L. Schoo, and M. Telszewski: An Enhanced Ocean Acidification Observing Network: From People to Technology to Data Synthesis and Information Exchange. Frontiers in Marine Science, 6, 337, DOI:10.3389/fmars.2019.00337, 2019.

Tilbrook, B, C. Neill and J. Akl: Surface water CO2 measurements from ships of opportunity: A report for Australia's Integrated Marine Observing System, 26 pp., doi: 10.25919/x90f-bw32, 2025.

Touratier, F., Azouzi, L., and Goyet, C.: CFC-11, Δ14C and 3H tracers as a means to assess anthropogenic CO2 concentrations in the ocean. Tellus B, 59(2), 318–325, doi:10.1111/j.1600-0889.2006.00247.x., 2007.

UNESCO, Tenth report of the Joint Panel on Oceanographic Tables and Standards. UNESCO Technical Papers in Marine Science. 1981.

Uppström, L. R.: The boron/chlorinity ratio of deep-sea water from the Pacific Ocean, Deep Sea Research and Oceanographic Abstracts, 21, 161–162, https://doi.org/10.1016/0011-7471(74)90074-6., 1974.

van Wijk, E. M., and Rintoul, S. R.: Freshening drives contraction of Antarctic bottom water in the Australian Antarctic Basin: Freshening drives contraction of AABW. Geophysical Research Letters, 41(5), 1657–1664. https://doi.org/10.1002/2013GL058921, 2014

Williams, G. D., Aoki, S., Jacobs, S. S., Rintoul, S. R., Tamura, T., and Bindoff, N. L.: Antarctic Bottom Water from the Adélie and George V Land coast, East Antarctica (140–149 E), J. Geophys. Res. Ocean., 115, C04027, https://doi.org/10.1029/2009JC005812, 2010.

Xue, L., Cai, W.-J., Takahashi, T., Gao, L., Wanninkhof, R., Wei, M., Li, K., Feng, L., and Yu, W.: Climatic modulation of surface acidification rates through summertime wind forcing in the Southern Ocean, Nat. Commun., 9, 3240, https://doi.org/10.1038/s41467-018-05443-7, 2018.

Zhang, S., Wu, Y., Cai, W.-J., Cai, W., Feely, R. A., Wang, Z., et al.: Transport of anthropogenic carbon from the Antarctic shelf to deep Southern Ocean triggers acidification. Global Biogeochemical Cycles, 37, e2023GB007921. https://doi.org/10.1029/2023GB007921, 2023.